Title page

Rapid quantification of fluorescent micro- and nanoplastics (⩽2 μm) in soil

Yin Liu[a]*, Junwei Hu[a]*, Patria Novita Kusumawardani[a], Stanislav Perevoschikov[b], Cao Lin[b], Shen Seselle [c], Steven Sleutel[a], Richard Hoogenboom[c], Andre Skirtach[b], Stefaan De Neve[a]

[a]Department of Environment, Faculty of Bioscience Engineering, Ghent University, 9000 Ghent, Belgium.

[b]Department of Biotechnology, Faculty of Bioscience Engineering, Ghent University, 9000 Ghent Belgium.

[c]Supramolecular Chemistry Group, Centre of Macromolecular Chemistry (CMaC), Department of Organic and Macromolecular Chemistry, Ghent University, Krijgslaan 281 S4, 9000 Ghent Belgium.

*Corresponding author, Yin.Liu@UGent.be, Junwei.hu@Ugent.be

Abstract

Micro- and nanoplastics (MNP) pose an emerging threat to soil ecosystems, with particular concern for small MNP (⩽10 μm). Although small fluorescent MNP are widely used to track MNP distribution and transport in aquatic environments and organisms, analyses of small fluorescent MNP in soil remain qualitative. Here, we present the first direct quantification approach for MNP ⩽ 2 μm in soil using fluorescence microscopy, with recoveries calculated from fluorescence area ratios between MNP in filtered soil suspensions and pure water. Direct detection yielded rapid and reliable quantification with recovery rates (49.1–53.1%) comparable to magnetic separation (60.4–61.7%) and about 7 times higher than conventional separation (6.8–7.5%). We established a robust calibration line (R^2 = 0.988) converting fluorescence area ratios to MP concentrations across a wide range (0.01–1000 mg/kg) in loamy sand, with systematic underestimation corrected through linear calibration. Under more realistic conditions (MP mixed with larger amounts of soil and incubated for 15 d), quantification yielded an average symmetric mean absolute percentage error ranging from 15% to 39%. The calibration curve was applicable across diverse soil types (R^2= 0.979-0.998) and MNP sizes down to 500 nm (R^2=0.961). This direct detection method provides a highly efficient, robust tool to advance mechanistic understanding of MNP behaviour and environmental hazards in soils.

Keywords: Microplastic and nanoplastic detection, fluorescent labelling, magnetic extraction, soil.

Synopsis

This study provides a methodology for quantitative direct detection (i.e. without extraction) of small fluorescent micro- and nanoplastics (MNP) across different soil types and MNP sizes (0.5-2 μm).

Graphical abstract

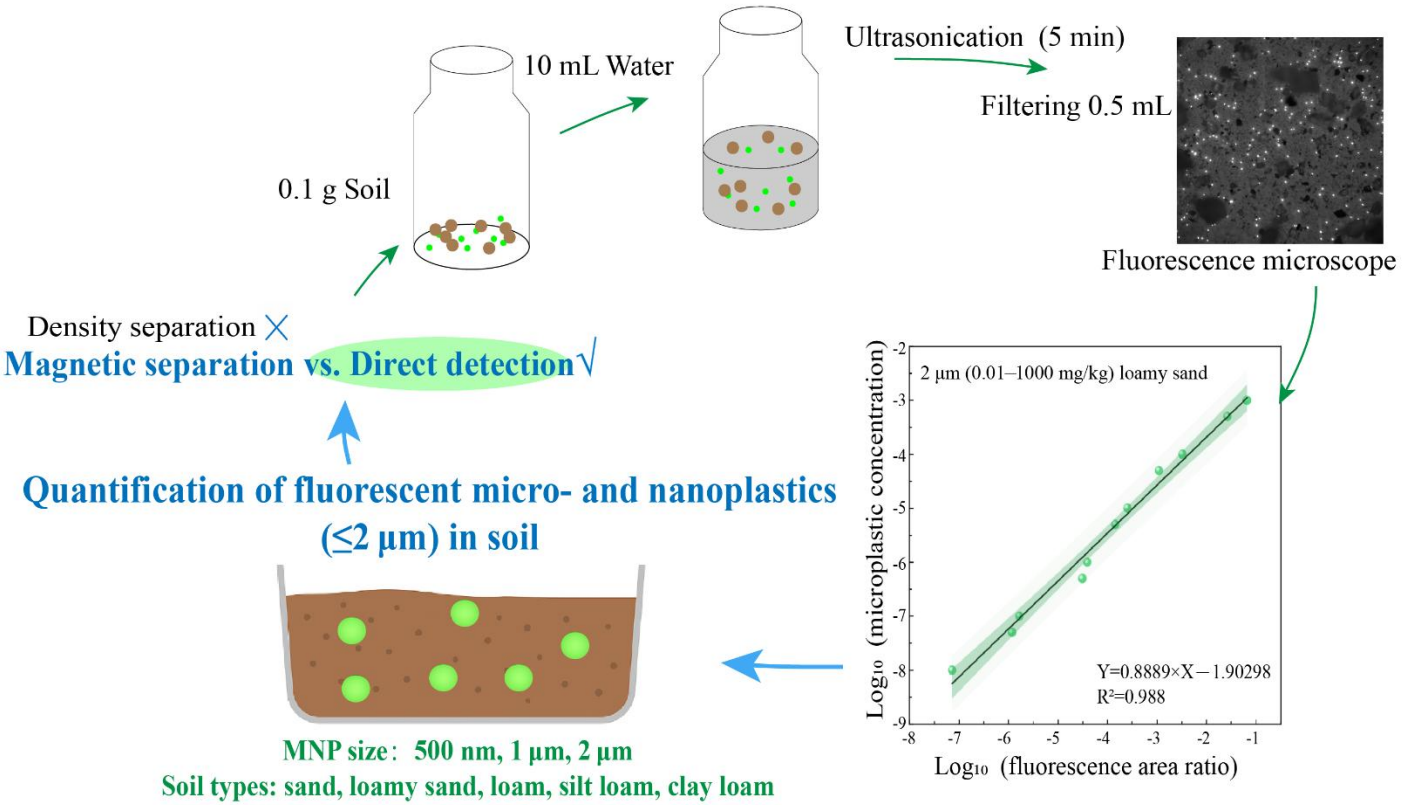

1. Introduction

Ubiquitously distributed plastic debris has emerged as a critical global pollutant, with particular concern regarding small-sized micro- and nanoplastics (MNP, ⩽ 10 μm).[1-3] Small-sized MNP are likely to remain a major intermediate form for extended periods due to continuous ageing and fragmentation, as MNP smaller than 1 mm are the most frequently detected size fraction in agricultural soils. [4-6] While research has mainly focused on aquatic systems, studies on MNP in soil started comparatively late and remain in their early stages [7, 8], even though most MNP are found in terrestrial ecosystems [9]. Small-sized MNP can be readily ingested by soil organisms, transferred through food chains, and penetrate biological barriers (e.g., cell membranes), ultimately threatening both ecosystem integrity and human health.[10, 11] For example, MNP⩽2 μm in soil can be actively ingested and transported by nematodes,[12, 13] and MNP⩽ 2 μm have been observed in plant roots and can be translocated to the aboveground part.[14-16] Small-sized MNP, with their extensive specific surface area and adsorption capacity, can serve as vectors for the transport of hazardous pollutants.[17, 18] Therefore, environmental concerns about MNP increase with decreasing MNP size, but the environmental behaviour of small-sized MNP remains poorly understood due to the lack of reliable methods for extraction, identification and quantification.[19]

Conventional MNP extraction (typically consisting of organic matter removal and density separation) is ineffective in separating small-sized MNP from soil due to the strong interactions between MNP and soil particles (particularly clay and organic matter).[20] E.g. Li et al. (2024) reported a 29% recovery rate for 10 μm PS MP in soil using density separation.[21] Identification of such small MNP extracted from soil is limited by the detection thresholds of Fourier-transform infrared (FTIR) spectroscopy (10 μm) and Raman spectroscopy (1 μm). In addition, spectroscopic identification is hindered by the fact that MP separation from soil is only partially effective, often resulting in weak spectral signals and poorly defined characteristic features.[22] Scanning electron microscopy coupled with energy-dispersive X-ray spectroscopy

(SEM-EDS) provides visual insights into the shape, size, and elemental composition of MNP, but is unrealistic for their quantification.[23] Alternatively, pyrolysis gas chromatography-mass spectrometry (py-GC/MS) in theory offers the possibility for direct detection of MP, but even there separation of MP from the soil matrix is needed for efficient detection.[21] Nanoparticle tracking analysis (NTA) allows quantification of MNP with a detection limit of 100 nm in relatively simple suspensions, but it struggles with chemical identification and is therefore difficult to apply to soils. [24] As a result, practical methods for accurately quantifying unlabelled MP in soils are limited to particles > 10 μm, leaving the environmentally most relevant fraction undetected. Monitoring dynamics of small MNP in soils therefore necessarily requires the labelling of these particles.

Labelling MNP with fluorescent dyes is an efficient, low-cost approach for tracking small-sized MNP and is mainly applied in aquatic environments and biota.[1, 25-30] Instruments used for imaging and manual or semi-automatic counting of fluorescent MNP include fluorescence microscopy and confocal laser scanning microscopy, NTA, and flow cytometry (FCM), amongst others.[29] The application of small-sized fluorescent MNP has remained very limited in sediments and soils.[29, 30] Only four studies used fluorescent MNP <10 μm in sediment, gravel and artificial soil, and only three in real soil, none of which reported quantification of the MNP (Table S1). Soil autofluorescence and physical encapsulation and adsorption of fluorescent MNP interfere with detection by increasing background signals and attenuating fluorescence intensity, highlighting the need for effective separation. However, again, conventional density-based separations are inadequate for isolating MNP smaller than 10 μm.

To circumvent the challenges of MNP separation from soil, magnetic separation may serve as an alternative to density separation to reduce background interference from soil. A recently developed magnetic extraction method, based on the attachment of magnetic nanoparticles to the MP surface followed by magnetic separation, achieved a recovery rate of 93% for 4 μm particles in sandy soil.[20] Nevertheless, the co-

labelling of soil particles during magnetic labelling of MP introduces challenges regarding the applicability of magnetic separation to smaller fluorescent MNP and further validation across diverse soil types is needed. An alternative that bypasses separation entirely is the direct detection of fluorescently labelled MNP in soil.[31] Here, direct detection is defined as the quantification of fluorescently labelled MNP in soil without any prior separation, based on fluorescence signals obtained directly from the sample. Sinha Ray et al. (2025) directly detected large polyethylene (PE) particles (425–500 μm) and PLA (250–300 μm) in loamy soil using a calibration relation between number or area of fluorescent particles and their concentration, achieving recoveries of 88 ± 35% (PE) and 82 ± 8% (PLA).[31] However, they further found that the spiked recovery decreased with decreasing MP particle size to 84 ± 3% for PE and 72 ± 16% for PLA in the 125–150 μm fraction,[31] likely because smaller MNP are more readily obscured or encapsulated by soil particles. These results indicate that the performance of direct detection is size-dependent, and its applicability to MNP ≤ 10 μm warrants further investigation.

Herein, building on our recent work, we set out to quantify small fluorescent MNP (⩽2 μm) in soil, using two detection strategies. We first tested the recovery rates of 2 μm fluorescent MP in loamy sand soil by 3 methods, namely conventional separation (density separation + organic matter removal), magnetic separation, and direct detection (no separation). Recovery was quantified based on MP fluorescence area ratios in soil relative to those in pure water controls. We then optimised the direct detection by comparing different data acquisition protocols to establish a reliable MP calibration curve, enabling the conversion of fluorescence area ratios into MP concentrations across a wide concentration range (0.01–1000 mg/kg). Direct detection was then used to quantify MNP for a range of soil types and MNP sizes. This study shows direct detection to be a highly efficient and robust method for quantifying fluorescent MNP ⩽2 μm in soil with potential broad applicability for studying MNP distribution, transport, and environmental fate.

2. Materials and methods

2.1. Materials

Green-fluorescent PS MP spheres with a diameter of 1.99±0.03 μm (PS-FluoGreen-W36), 1.09±0.03 μm (PS-FluoGreen-Fi330-1), 0.563±0.01 μm (PS-FluoGreen-Fi297) with an excitation wavelength of 502 nm and an emission wavelength of 518 nm, were purchased from Microparticles GmbH (Berlin, Germany) as a suspension with 2.5% w/w MNP concentration. Iron (III) chloride hexahydrate ($FeCl_3 \cdot 6H_2O$) (Lot# 087K0204) and iron (II) chloride ($FeCl_2$) (Lot# MKCB2626V), purchased from Sigma-Aldrich Chemie GmbH (Steinheim, Germany), were used for magnetic nanoparticles synthesis for magnetic separation, according to our previous research (synthesis steps in Text S1). A nickel-plated neodymium magnet (model Q-51-51-25-N, manufactured by Webcraft GmbH, Germany) with a magnetic force of 100 kg at zero working distance was used for magnetic extraction. Whatman™ membranes (diameter 25 mm, mixed cellulose ester) with pore sizes of 0.45 μm and 0.2 μm were purchased from Sigma-Aldrich Chemie GmbH (Germany). Five soils with contrasting textures (sand, loamy sand, loam, silt loam, and clay loam) were collected in East Flanders, Belgium (Table 1). The fresh soil was air-dried and sieved through a 2 mm mesh screen to remove stones and roots.

Table 1

Basic properties of the soils used in this research.

Soil type	Sand %	Silt %	Clay %	Location	Coordinate	Depth	Soil organic carbon %	pH-KCl
Sand	89.5	7.4	3.2	Beernem, East Flanders, Belgium,	51°06'41.2"N 3°19'03.1"E	0 – 15 cm	0.56	4.24
Loamy sand	79.7	17.4	3.0	Kruisem, East Flanders, Belgium	50°55′48.5″N 3°33′06.7″E	0 – 15 cm	0.9	5.11
Loam	48.6	43.6	7.7	Oosterzele, East Flanders, Belgium	50°57′39.6″N 3°45′59.3″E	0 – 15 cm	1.11	6.16
Silt loam 1	17.8	67.5	14.8	Oosterzele, East Flanders, Belgium	50°55′17.1″N 3°45′01.4″E	0–30	1.62	6.37
Silt loam 2	36.2	52.8	11.0	Oosterzele, East Flanders, Belgium	50°55′10.6″N 3°45′09.1″E	30–50 cm	0.56	6.70
Silt loam 3	12.9	76.3	10.8	Oosterzele, East Flanders, Belgium	50°55′17.1″N 3°45′01.7″E	0 – 15 cm	1.54	6.00
Clay loam	34.0	31.0	35.0	Bottelare, East Flanders, Belgium	50°39′29.4″N 3°46′05.3″E	40–60 cm	0.16	5.91

2.2. Experiment I: Method comparison

The optimal quantification of fluorescent MNP (⩽2 μm) in soil was investigated through 3 methods, as summarised in Table 2. For each method, two MP concentrations, namely 10 and 100 mg/kg, corresponding to 2.27×10^{9} and 2.27×10^{10} items of 2 μm MP per kg soil, respectively, were used, each in three replicates (n=3). To achieve these concentrations, 40 μL and 400 μL of a 2.5×10^{-5} (w/w) MP suspension were separately added to 0.1 g of air-dried soil and mixed manually.

2.2.1. Density separation (Figure 1a) and magnetic separation (Figure 1b)

The density separation procedure was carried out according to a conventional MP detection method (detailed steps in Text S2).[18] The magnetic extraction was done

according to our previous study with some modifications.[20] Briefly, MP were heated to near their glass transition temperature (T_g) in a suspension containing Fe_3O_4 nanoparticles, allowing the nanoparticles to adhere to the MP surface, which were then fixed upon cooling, allowing extraction by a magnet (see [20] for details). To avoid alterations to the magnetic nanoparticle properties at high temperatures, we modified the original procedure by first heating MP to near their T_g and then adding the magnetic nanoparticles. Furthermore, the extraction was repeated two more times (3 extraction steps as compared to a single extraction in the original procedure) because loamy sand resulted in high soil co-labelling (detailed steps in Text S3).

2.2.2. Direct detection/no extraction (Figure 1c)

In the direct detection method, MNP in a very thin soil layer are directly detected using fluorescence microscopy. Soil layers with relatively low surface roughness facilitate accurate focusing during fluorescence microscopy, maximising particle recovery. The fluorescence ratio of the MP visible at or near the soil surface is expected to correlate with MP concentration in the entire soil volume. To obtain a homogenous MP distribution in the soil suspension, the mixtures of MP and soil were dispersed by addition of 10 mL of pure water (soil-to-water ratio of 1:100), followed by ultrasonication for 5 min (Bandelin Sonorex Super 10P DK 255 P Ultrasonic Bath, 100% power, 20°C) and manual shaking. Then, a 0.5 mL aliquot (thus containing 5 µg of soil) was taken and filtered through a 0.45 µm filter paper. The filtration procedure was preceded by the addition of 2 mL of ultrapure water to the filter funnel, followed by 0.5 mL of the test suspension and another 2 mL of ultrapure water to promote particle dispersion, after which the vacuum pump was activated. After air-drying, the filter paper was flattened and fixed with a coverslip for fluorescence microscopy analysis. Assuming an average soil particle density of 2.65 g/cm³, the calculated thickness of a hypothetical continuous “soil layer” of this mass (5 µg) with 20% of pore space would be around 10µm. However, the microtopography of such “soil layer” will differ greatly depending mainly on soil texture. For e.g. the loamy sand soil, it will be mostly

discontinuous with “large” isolated sand particles (50-2000 µm, greatly exceeding the average 10 µm thickness) interspaced with uncovered areas of the filter, resulting in a very pronounced microtopography (as discussed in section 4.3.1). Yet also for this loamy sand [32], the focal plane in which most 2 µm MP settle was observed to be variable yet sufficiently thin to reduce the likelihood of MP being embedded in or obscured by soil particles.

2.2.3. MP detection and quantification

For all 3 MP separation/detection methods, the MP recovery rates were calculated as the ratio of the fluorescence area ratio of MP extracted from soil, or directly detected in soil, to that of pure MP (without soil) at the same MP addition rate. To this end, an amount of MP corresponding to 10 and 100 mg/kg was dispersed in 10 mL of ultrapure water using ultrasonication for 5 min (three replicates, n=3). A 0.5 mL aliquot was then taken and filtered through a 0.45 µm filter paper for fluorescent area detection. The precision of the different methods was evaluated by calculating the relative standard deviation (RSD) of the MP recovery rates.

The MP could be identified and photographed (at ×20 objective lens) on the filter paper using a fluorescence microscope (Nikon Eclipse Ti2-Widefield, Total Internal Reflection Fluorescence microscopy). To ensure consistency in fluorescence images, the imaging settings of the fluorescence microscope were standardised, with the laser power at the excitation wavelength set to level 3 and the exposure time fixed at 35 ms. The focus was then fine-tuned to capture MP fluorescence in the clearest, smallest possible area with the highest intensity. A total of 50 images (accounting for 15.92% of the filter area) were randomly photographed. All captured images were processed semi-automatically using ImageJ macro and batch processing (version 1.54g) to calculate the fluorescence area ratio of each image, with the colour thresholding in ImageJ set from 229 to 255. For each filter, the fluorescence area ratio per image was represented as boxplots using SPSS to identify outliers. Outliers were removed only if they resulted from incorrect recognition caused by background interference in ImageJ.

2.3. Experiment II: Optimisation of the direct detection

2.3.1. Establishing calibration curve (Table 2, IIA)

To establish a robust calibration curve, the data acquisition procedure was first optimised by assessing the effect of the number of replicate samples (1, 2, and 3), the number of subsamples per replicate (1, 2, and 3), and the number of images per filter (10, 20, 30, 40, and 50) on the Pearson correlation coefficient (r) of the calibration curve using a resampling approach (detailed description in Text S4 and Figure S1). Based on a combination of simplicity and accuracy, the optimum procedure selected was to use a single sample with a single subsample per concentration, and this procedure was then used consistently for establishing the calibration curves. Briefly, eleven concentrations of 2 μm MP (0.01, 0.05, 0.1, 0.5, 1, 5, 10, 50, 100, 500, and 1000 mg/kg) were individually mixed with 0.1 g of loamy sand. For each concentration, 30 images per filter were acquired. If fewer than two fluorescent particles were detected within these 30 images, the number of images was increased to 150 to improve detection accuracy at low MP concentrations. The mean fluorescence area ratio per image was calculated, and MP concentrations were converted to percentages to obtain dimensionless values. A linear relationship between the base-10 logarithms of fluorescence area ratio and MP concentration was established to construct the calibration curve.

2.3.2. Extension of the calibration-based quantification (Table 2, IIB)

The mixing of a very small amount of soil with MP, immediately followed by direct detection of the MP in the mixture represents simplified conditions. Therefore, more realistic conditions were imposed by using larger amounts of soil and an incubation of the soil+MP mixture prior to direct detection. Fluorescent MP (2 μm) were mixed with 5 g of loamy sand at concentrations of 1 and 100 mg/kg, respectively, in three replicates. The soil moisture content was adjusted to 17.07% (WFPS 55%), and the soil+MP mixtures were incubated at a constant temperature of 20°C for 15 d. After incubation, the soil was air-dried, soil aggregates were gently crushed using a stainless steel spatula, the soil was thoroughly mixed, and transferred into 20 mL glass vials. The soil was

253 further homogenised by shaking at 300 rpm for 30 min, and a 0.1 g replicate sample
254 was taken for direct detection following the methodology described in section 2.2.2.
255 Further experiments were conducted to evaluate whether increasing the number of
256 replicate samples and the soil-to-water ratio could improve analytical accuracy
257 (schematic illustration in Figure S2). To evaluate the calibration-based quantification
258 calibration curve, mean absolute error (MAE), root mean square error (RMSE), and the
259 average symmetric mean absolute percentage error (SMAPE) were calculated (details
260 provided in Text S5).

2.4. Experiment III: Direct MNP detection in various soil types and different MNP sizes

2.4.1. Various soil types (Table 2, IIIA and B)

The direct detection method was further applied in seven soils with varying texture: sand, loamy sand, loam, three silt loams (further denoted as silt loam1, 2 and 3), and clay loam, with calibration curves established following the methodology described in section 2.3.1.

For two of these soils (silt loam 1 and clay loam) MP quantification using larger amounts of soil and pre-incubation as described in section 2.3.2 was also performed.

2.4.2. Various MNP sizes (Table 2, IIIC)

Fluorescent MNP of 500 nm and 1 μm were individually mixed with 0.1 g of loamy sand at 11 concentrations (0.01, 0.05, 0.1, 0.5, 1, 5, 10, 50, 100, 500, and 1000 mg/kg). The calibration curve was then established following the methodology described in section 2.3.1. For the detection of 500 nm NP, a smaller 0.2 μm filter was used instead of 0.45 μm. Due to the smaller particle size, the fluorescence microscope was configured with a ×60 objective lens, an exposure time of 100 ms, and an excitation laser intensity of 10. Imaging of fluorescent NP was performed promptly (within ~5 s) to minimise photobleaching.

Table 2

The objectives, experimental factors considered, levels of the experimental factors of the spiking experiments, and the optimal parameters

Experiments/Objectives	Factors	Treatments/Levels	MP concentrations	MNP size	Replicate samples	Subsamples	Image number	Soil types	Manuscript section
I: Method comparison	Extraction or direct detection	Density separation, magnetic separation, and direct detection	10 and 100 mg/kg	2 µm	3	1	50	Loamy sand	2.2
II: Optimisation of direct detection	IIA: Calibration	Sample, subsample, and image numbers	0.01, 0.05, 0.1, 0.5, 1, 5, 10, 50, 100, 500, and 1000 mg/kg	2 µm	1	1	30 or 150 at low concentration	Loamy sand	2.3.1
	IIB: Larger amount of soil + 15 d pre-incubation	Sample numbers and different soil-to-water ratios	1 and 100 mg/kg	2 µm	3 or 9	1	30	Loamy sand	2.3.2
III: Application of direct detection	IIIA: Calibration curve across various soil types	Soil types	0.01, 0.05, 0.1, 0.5, 1, 5, 10, 50, 100, 500, and 1000 mg/kg	2 µm	1	1	30	Sand, loamy sand, loam, silt loam 1, silt loam 2, silt loam 3, and clay loam.	2.4.1
	IIIB: Larger amount of soil + 15 d pre-incubation	Soil types	1 and 100 mg/kg	2 µm	3	1	30	Silt loam 1 and clay loam.	2.4.1
	IIIC: Calibration curve across various MNP sizes	MNP size	0.01, 0.05, 0.1, 0.5, 1, 5, 10, 50, 100, 500, and 1000 mg/kg	1 µm and 500 nm	1	1	30	Loamy sand	2.4.2

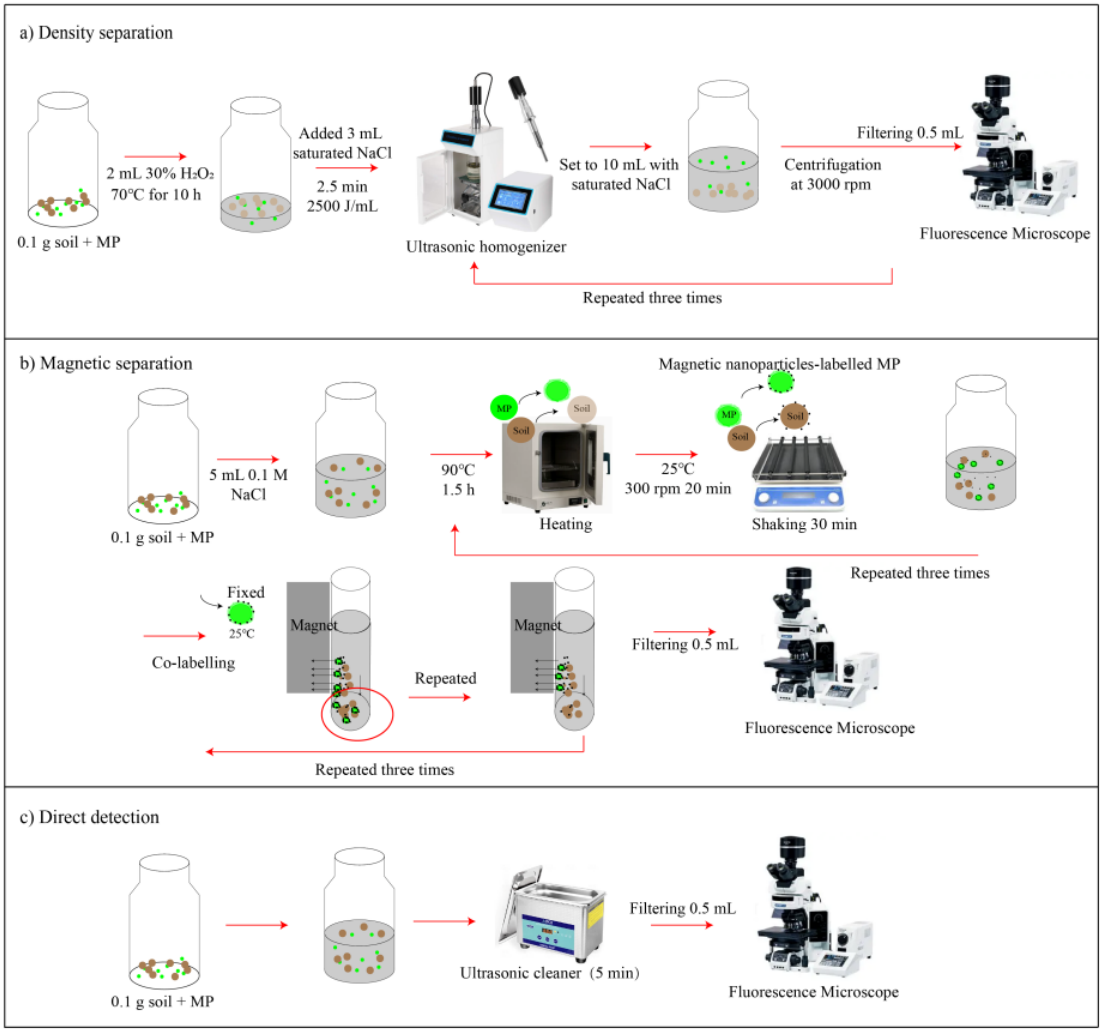

Figure 1. Schematic diagram of density separation, magnetic separation, and direct detection of MP in loamy sand soil.

3. Results

3.1. Separation or no separation

Direct detection achieved recoveries of 49.1 ± 9.3% at 100 mg/kg and 53.1 ± 10.9% at 10 mg/kg, which were comparable to those obtained by magnetic separation (60.4 ± 5.0% and 61.7 ± 3.2%), and 6.5–7.8 times higher than those achieved by conventional separation (7.5 ± 2.3% and 6.8 ± 0.8%) (Figure 2). Although magnetic separation showed slightly better precision (RSD: 8.3% at 100 mg/kg and 5.1% at 10 mg/kg) than direct detection (RSD: 18.8% at 100 mg/kg and 20.5% at 10 mg/kg), both methods demonstrated acceptable reproducibility. Notably, direct detection was by far the most time-efficient approach, requiring only ~7 min of preparation per 0.1 g soil sample (5 min for soil dispersion and 2 min for filtration), whereas magnetic separation required nearly 9 h and conventional separation required 15 h.

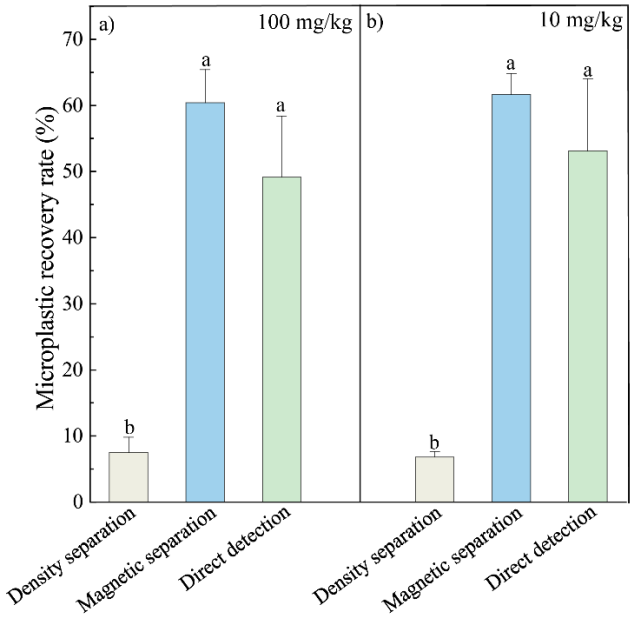

Figure 2. The recovery rate of density separation, magnetic separation, and direct detection. Treatments without shared letters indicate a significant difference (p-value < 0.05), tested by One-way ANOVA.

3.2. Optimisation of the direct detection

3.2.1. Data acquisition protocols used for the calibration curve

The calibration curve showed a strong linear relationship between the $\log_{10}$-transformed fluorescence area and MP concentration ($R^2 = 0.988$, Figure 3a), with slight deviations observed at low concentrations (<1 mg/kg). No significant decrease in r was observed when subsamples (a 0.5 mL aliquot was taken from the total 10 mL soil suspension) were reduced from 3 to 1 (Table S3). Increasing the number of replicate samples (0.1 g soil spiked with MP) and images per filter both slightly increased the r value and LDC. For 11 MP concentrations, one replicate sample subsampled only once was prepared, and 30 images per filter were initially acquired. This dataset was sufficient to establish a strong positive correlation at 0.05 mg/kg LDC, with an average r value of 0.995 ± 0.003 across 25 sampling iterations (Table S2). However, for a low MP concentration range, the number of analysed images for filter paper samples affects the LDC. Therefore, if fewer than two fluorescent particles were detected among the initial 30 images, the number of captured images was increased to 150 to enable LDC down to 0.01 mg/kg.

3.2.2. Extension of the calibration-based quantification

For the larger amount of soil combined with pre-incubation, a single replicate sample from each of the three incubation replicates yielded relatively low SMAPE values of 28% at 100 mg/kg and 17% at 1 mg/kg MP (Figure 3h and Table S4). Increasing the number of replicate samples per incubation replicate did not significantly increase the accuracy. Increasing the soil-to-water ratio to 10:1 reduced detection accuracy. In addition, with the same samples and soil-to-water ratios, the SMAPE values at 1 mg/kg were consistently lower than those at 100 mg/kg (Table S4).

3.3. Application of direct detection in varying soil types and MNP sizes.

3.3.1. Varying soil types

Strong linear correlations between fluorescence area ratios and MP concentrations were observed in all soils, with R^2 ranging from 0.979 in silt loam 1 to 0.998 in sand

(Figure 3a–g). The largest deviations from the regression line were observed in all three silt loam soils, most notably at concentrations below 1 mg/kg. The R^2 values of the calibration curves showed a statistically significant negative correlation only with soil pH ($r = –0.761$, $p < 0.05$) (Table S5). In addition, there was a marginally significant negative correlation between R^2 values and silt content ($r = –0.717$, $p = 0.07$). Soil pH, fluorescence area ratio, silt content, and sand content also displayed significant pairwise correlations.

Despite yielding the lowest R^2 among all soil types, the calibration curve in silt loam 1 still provided acceptable MP detection accuracy, with SMAPE values of 4% at 100 mg/kg and 38% at 1 mg/kg. Clay loam soil exhibited elevated SMAPE values of 96% at 100 mg/kg and 71% at 1 mg/kg, despite yielding a relatively high R^2 (Figure 3h).

3.3.2. Calibration curves for different MNP sizes

A strong linear relationship was observed between the fluorescence area ratio and the concentration of 1 μm MP ($R^2 = 0.989$, Figure 4a), whereas this relationship was slightly weaker for 500 nm NP ($R^2 = 0.961$, Figure 4b). Images at 500 and 1000 mg/kg NP were excluded because overlapping fluorescence and excessive signal intensity impeded accurate focusing. Notably, fluorescence photobleaching was significant during NP detection, with the fluorescence intensity at the same imaging spot decreasing substantially within 10 min of continuous observation (Figure S3). To minimise photobleaching, fluorescent NP imaging was performed rapidly (approximately 5 s) and avoiding repeated imaging of the same region.

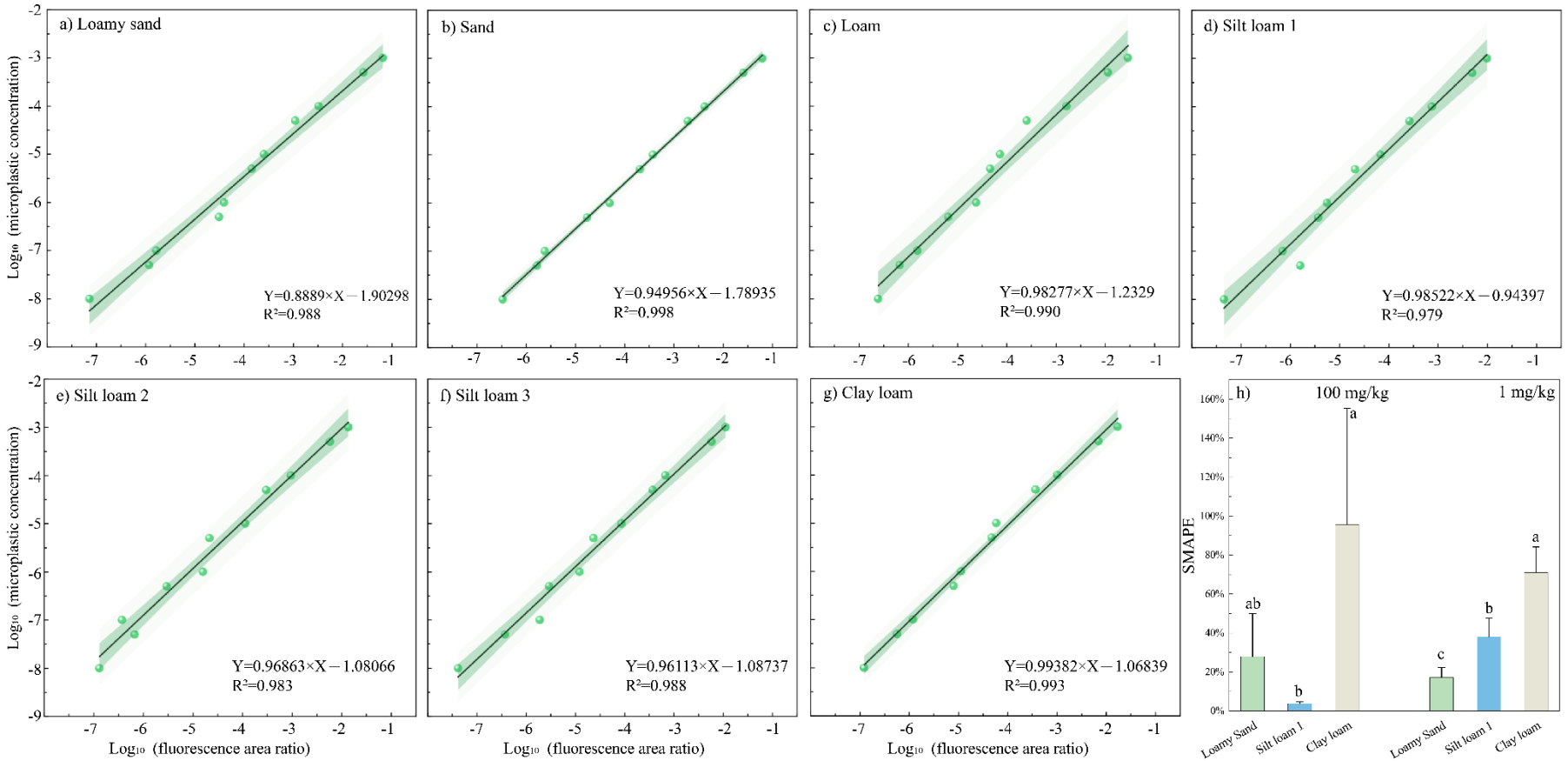

Figure 3. Linear correlation of fluorescence area ratio versus MP concentration across soil types (a–g); Evaluation of the calibration-based quantification for loamy sand, silt loam 1, and clay loam during a 15-day incubation (h). Error bars indicate standard deviation. Treatments without shared letters indicate a significant difference (p-value < 0.05), tested by One-way ANOVA.

354

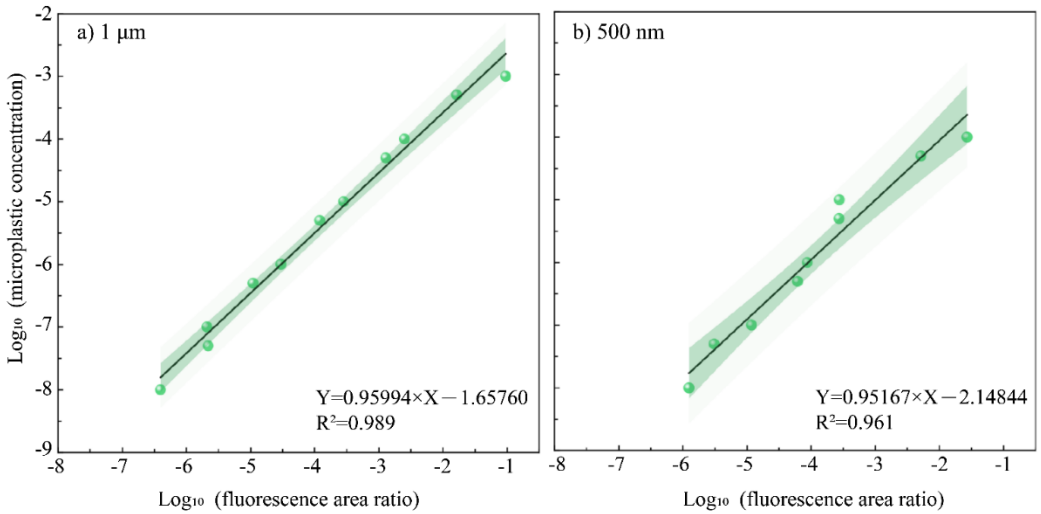

355

356 **Figure 4.** Linear correlation between fluorescence area ratio and MP concentrations in various MNP sizes.

4. Discussion

4.1. Performance of direct detection versus separation methods

Quantifying small MNP in soil remains challenging because of the inefficient extraction and detection, and using fluorescent MNP has been shown to provide a promising alternative for mechanistic studies.[29] We systematically compared conventional separation (combination of organic matter removal and density separation), magnetic separation, and direct detection, in terms of recovery, precision, efficiency, and applicability for the quantification of fluorescent MNP in soil (Table 4). The very low recovery rate of conventional separation (6.8–7.5%) confirms that current conventional separation methods cannot be used for quantification of small MNP. About 50% of the MP remained undetected with direct detection, which can be explained by (i) the uneven soil surface (on the microscale) on the filter leading to focal-plane mismatch and fluorescence blurring; (ii) the shielding of MNP by soil particles; [31] (iii) MNP aggregation and MNP particle overlap during filtration. The RSD of direct detection (18.8–20.5%, which can be considered low for MP of this size class) partly results from the intrinsic self-aggregation of MP, leading to non-uniform spiking among replicates.[20, 33, 34] Despite measures being taken to minimise non-uniform spiking, including freshly preparing MP suspensions directly before use, applying ultrasonic dispersion, and using glass containers to reduce interactions between MP and container walls, the RSD for 100 mg/kg MNP in ultrapure water was still 11.5%. In addition, MP are not uniformly distributed on the filter paper, so random image selection inevitably introduces additional variability. In contrast, magnetic separation eliminates most coarse minerals and part of the organic matter, improving particle dispersion and thereby enhancing accuracy and precision.[20] Overall, direct detection shows great potential for MNP quantification, with systematic underestimation inherently accounted for in the calibration as discussed in section 4.2.

Importantly, the main advantage of direct detection lies in its substantially higher efficiency and broader applicability compared with separation-based methods (Table

385 3). Sample preparation for direct detection of fluorescent MNP requires only
386 approximately 7 min, i.e. two orders of magnitude faster than separation-based methods.
387 Direct detection is based on the inherent fluorescence of covalently labelled MP,
388 avoiding the co-labelling challenges of the magnetic separation, leading to high
389 efficiency and broad applicability across soil types and MNP size, as verified in section
390 3.3. Direct detection is thus the method to be recommended for quantifying fluorescent
391 MNP in soil.
392
393 **Table 3**
394 Comparison of advantages and disadvantages of direct microscopy detection and
395 separation-based detection for quantification of fluorescent MNP < 2 μm in soil.

Aspects of comparison	Direct detection	Magnetic separation	Density separation
Accuracy (Recovery rate)	High (49.1–53.1%)	High (60.4–61.7%)	Low (6.8–7.5%)
Precision (RSD)	Relatively high (18.8–20.5%)	High (5.1–8.3%)	Relatively high (1.8–30.7%)
Sample preparation time	~7 min	~9 h	~15 h
Co-labelling interference	None	High	None
Applicable to a variety of soil types	High	Need further validation	Low
NP detection	Yes	Need further validation	No
Applicable to various plastic types and shapes	High potential	Need further validation	Yes

396 Recovery rate and the relative standard deviation (RSD) data obtained from the quantification of 2 μm
397 MP in loamy sand.
398
399 **4.2. Optimization of the direct detection**
400 4.2.1. Data acquisition protocols for calibration curve
401 Following a comparison of datasets varying in the number of replicate samples,
402 subsamples per replicate, and images captured per filter paper, the established data
403 acquisition protocol reliably produced strong linear relationships between fluorescence
404 area ratio and MNP concentration in loamy sand ($R^2 = 0.988$). The resulting calibration

405 curve indicates that the observed systematic underestimation (recovery ~50% of MP)
406 is highly reproducible and consistent across concentrations, and can be reliably
407 accounted for. No significant decrease in r was observed when the number of
408 subsamples (i.e. the 0.5 mL aliquot taken from the 10 mL soil suspension) was reduced
409 from 3 to 1 (Table S3), indicating that 5 min of ultrasonication was sufficient to
410 effectively disperse the MP before filtering. Increasing the number of replicate samples
411 (0.1 g soil spiked with MP) and images for fluorescence signal extraction per filter both
412 increased the r value (Table S3), indicating that non-uniform MP spiking across
413 samples and uneven MP distribution on the filter affected detection accuracy. At low
414 MP concentrations (MP$\leqslant$0.05 mg/kg), the number of images became the main factor
415 influencing the LDC. To minimise the workload when applying this method in practice,
416 the standard protocol (1 sample, 30 images) could first be employed, and only for those
417 samples where concentrations fall below 1 mg/kg soil, the number of replicate samples
418 and images could be increased to maximise detection accuracy. High r and
419 reproducibility are essential for reliable calibration, while data acquisition settings may
420 be adapted to different experimental conditions. Further optimisation may be achieved
421 by refining magnification settings, image recognition, image parameter extraction, and
422 model selection for calibration curve development.

423 4.2.2. Evaluation of the calibration-based quantification

424 Recent studies have predominantly optimised the quantification of MP in soils and
425 sediments for MP in the hundreds of micrometre size range [31, 35, 36], with some
426 studies focusing on 20–100 μm [34, 37], and limited attention given to the ~10 μm size
427 range [38, 39]. For the detection of MP below 5 μm in complex matrices, analytical
428 difficulty increases markedly with each micrometre decrease in size. Given the limited
429 knowledge of small-sized MP, especially with respect to their environmental fate and
430 associated risks, increased research attention should be directed toward smaller-sized
431 MNP. Here, we demonstrated that direct detection by fluorescence microscopy is an
432 accurate quantification method for small MNP. A single soil sample from each of the

three incubation replicates yielded relatively low SMAPE values of 28% at 100 mg/kg and 17% at 1 mg/kg for small-sized MP detection (Table S5). To further contextualise these results, we tried to compare our direct microscopic detection method with other potential fluorescent detection approaches. To the best of our knowledge, only one study has reported alternative quantitative approaches, using monodisperse MP/NP suspensions analysed by FCM or NTA in pure clay (bentonite, montmorillonite, kaolinite). [40] However, NTA is limited to detecting particles < 0.5 μm and with substantial quantification errors (e.g. percentage errors ranging from 172% to 473% for pure 500 nm fluorescent NP in deionized water). FCM generally provides more accurate and consistent results than NTA, with percentage errors typically remaining within ~40% across most tested concentrations for 0.5 and 1 μm PS in pure clay. [40] However, although FCM can accurately distinguish fluorescence MNP from clay particles, further validation in real soils would be needed. [40] In addition, the applicable size ranges of FCM are limited to > 0.5 μm. Our direct microscopy detection reliably quantified particles down to 500 μm, but advances in optical super-resolution microscopy (SRM) enable imaging down to tens of nanometres [41], offering new opportunities for direct detection in the smaller NP size range (<0.5 μm). Overall, direct microscopy detection imposes fewer constraints on MNP particle size, is simpler and broadly applicable across a broad range of soils.

The detection error caused by the mixing homogeneity may be limited in loamy sand, as increasing the number of replicate samples from each incubation replicate did not substantially reduce SMAPE, indicating minimal sample-to-sample variation (Table S4). Intuitively, increasing the soil-to-water ratio would be expected (given the increased soil mass) to increase sample representativity and measuring accuracy at low MP concentrations. However, a lower soil-to-water ratio resulted in lower SMAPE values at both 100 mg/kg and 1 mg/kg (Figure 3d). This may be explained by reduced self-aggregation of MP and a more uniform MP distribution on the filter paper at low soil-to-water ratios. Therefore, this ratio was not increased in subsequent analyses. Self-

aggregation of MP likely also explains why the SMAPE values observed at 1 mg/kg were consistently lower than those at 100 mg/kg (Figure 3d). In view of this, further optimisation may rather be achieved by further reducing the soil-to-water ratio and appropriately increasing sample size.

4.3. Applicable range of the direct detection method

4.3.1. Applicability in different soil types

Any MNP quantification method can only gain wide applicability when it is robust and can be used reliably in a wide range of soils. Direct detection proved to be a robust method, yielding highly linear calibration curves with relatively high R^2 across a wide range of soils with contrasting texture, SOM and pH (Figure 4a–f).

Both R^2 and the MP fluorescence area ratio were negatively correlated with silt content and positively correlated with sand content [42], and the possible reasons for this are further explored below. MP imaged under the microscope (Figure 5a–f) can be situated on the filter surface, within soil pores, or attached to soil particles (Figure 5g). Given the large density differences between mineral soil particles (typically 2.65 g/cm^3) and MP (non-colloidal) mineral particles settle onto the filter paper first during filtration. In sandy soil, the larger particle size results in low particle density on the filter paper, leaving large areas uncovered, thus increasing the likelihood of MP being directly exposed on the filter surface, thereby increasing the measured fluorescence area. Because of the expected slow settling rate of the colloidal clay particles, we hypothesised that MP recovery would decrease with increasing clay content, because MP would be covered by the settling clay particles. Possibly the vacuum applied during filtration causes clay particles to aggregate instantaneously, leading to rapid settling and a relatively smooth contiguous surface on top of which MP particles would settle, minimising physical shielding. This may explain why there was no significant reduction in MP recovery in the clay loam. In contrast, the silt-loam, the much stronger surface microtopography, results in a much more pronounced vertical distribution of the MP and stronger physical shielding, reducing the fluorescence area in the focal plane. Thus,

soil surface microtopography modulates the degree of MP shielding, thereby influencing fluorescence area and R^2. To mitigate these effects, especially in soils with high silt content, direct detection could be optimised by further reducing the soil layer thickness through a lower soil-to-water ratio.

R^2 and fluorescence area ratios also exhibited a significant negative correlation with soil pH (Table S5), which seems inconsistent with theoretical considerations. Previous studies have demonstrated that soils with lower pH values tend to exhibit a stronger adsorption capacity toward MNP [43, 44] and can facilitate the self-aggregation of MP. Under low pH, the surface charge of negatively charged MP is partially neutralised, thereby weakening electrostatic repulsion. Both enhanced soil adsorption and MP self-aggregation would thus be expected to reduce R^2 and fluorescence area ratios in low-pH soils, contrary to what we observed. Given that soil pH was significantly correlated with sand and silt contents (Table S5), the observed relationship between pH and R^2 is thus probably an indirect relation with soil texture.

The calibration curve established under more realistic conditions (larger amounts of soil, incubated for 15 d) showed that the silt loam 1, despite its lower R^2 of 0.976 as compared the clay soil (R^2 of 0.993), had higher detection accuracy, with SMAPE values of 4 ± 1% at 100 mg/kg and 38 ± 10% at 1 mg/kg, than the clay soil (e.g. SMAPE value of 96 ± 60% at 100 mg/kg). This may be due to the difficulty of achieving homogeneous mixing in clay-rich soils during both spiking and subsequent mixing. For clay-rich soils, better mixing of soil and MNP, as well as increasing the number of replicate samples, may help improve detection accuracy.

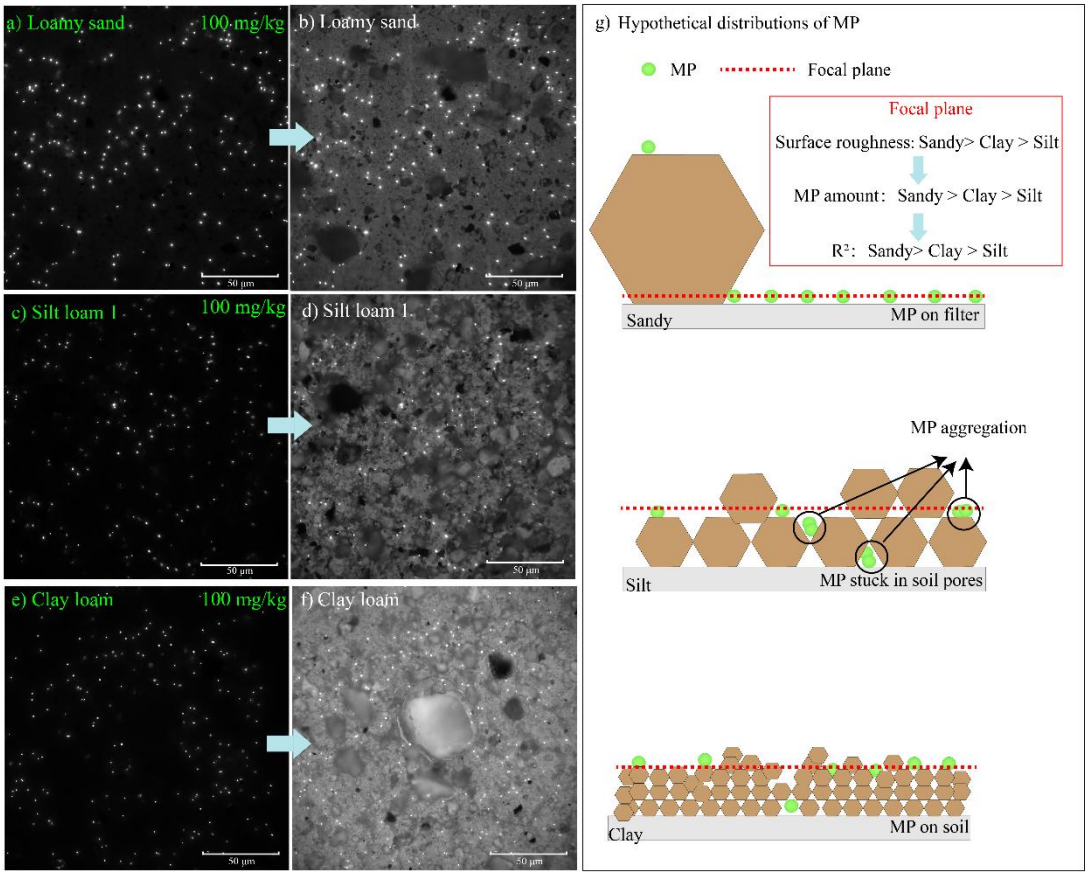

511

512 **Figure 5.** Direct microscopy of fluorescent MP in loamy sand, silt loam 1, and clay
513 loam at 100 mg/kg MP concentration: fluorescence images (a, c, and e) and
514 corresponding combined bright-field and fluorescence images (b, d, and f). g)
515 Hypothetical distributions of MP across different soil particles.

516

517 4.3.2. Applicability over MNP size classes

518 Our direct detection method allowed quantification of MP as small as 500 nm (R^2
519 = 0.961). Before this study, Palladium (Pd) core-doped NP coupled with ICP–MS
520 detection represented one of the few practically quantitative approaches for NP analysis
521 in real soils.[45], achieving 91% recovery. However, Pd doping of NP is costly and
522 labour-intensive in both particle synthesis and detection. And these particles cannot be
523 directly visualised. Beyond metal-doped approaches, quantification of isotope- and
524 radioisotope-labelled NP in complex soil matrices is further constrained by specialised
525 instrumentation requirements and, in the case of radioisotope-based methods, stringent

526 regulatory and radiological safety considerations. In contrast, fluorescent NP are readily
527 available and can be measured in a straightforward manner through simple imaging.
528 Moreover, because it relies on optical imaging, direct detection could potentially be
529 extended to smaller nanoparticles through advanced fluorescence techniques such as
530 stimulated emission depletion (STED) microscopy, which has been applied for
531 qualitative visualisation of 50 nm NP within nematodes.[46, 47] Therefore, direct
532 detection has the potential to greatly advance our understanding of NP distribution,
533 accumulation, and bioavailability.

534 The decreasing R^2 with decreasing NP size in this study (Figure 4) may result from
535 multiple factors. First, the small NP size and increasing discrepancy in size with soil
536 mineral particles make it less likely that the NP are positioned within the same focal
537 plane. Second, NP have a stronger tendency to aggregate than MP.[48] Third, the higher
538 magnification reduces the detection area. Direct NP detection could further be
539 optimised by e.g. further reducing the thickness of the soil layer on the filter and
540 increasing the number of images. In addition, the susceptibility of fluorescent labels to
541 photobleaching and fluorescence quenching is plastic type dependent and increases
542 with decreasing MNP size. [49-51] NP fluorescence intensity at a given imaging site
543 markedly decreased over 10 min of continuous observation (Figure S3). In order to
544 minimise photobleaching, fluorescent NP imaging is therefore recommended to be
545 conducted promptly, within about 5 s, while avoiding repeated imaging of the same
546 region. NP labelled with photostable fluorescent probes, such as carbon quantum dots,
547 may provide a more robust alternative.[52] Strategies to improve the fluorescence
548 stability of nanoparticles have been widely explored in biofluorescence imaging. [53,
549 54] However, such modifications should not substantially alter the physicochemical
550 properties of NP. For example, while SiO_2 encapsulation enhances photostability, it
551 may also significantly modify the original surface chemistry and behaviour of NP.[55]

552 **4.4. Environmental implications and limitations**

553 Given the current lack of reliable methods for quantifying small MNP in soils,

fluorescence labelling of MNP has been proven a necessary approach for advancing mechanistic understanding of MNP dynamics. Direct detection provides clear advantages for laboratory-scale studies of fluorescent MNP. First, it addresses the key challenge of reliably quantifying small-sized fluorescent MNP down to 500 nm in real soil environments. Second, direct detection reduces time and uncertainty from complex sample preparation, offering a practical and scalable approach that renders separation fundamentally unnecessary for fluorescent MNP quantification. Third, the robustness of the method across diverse soil types suggests its potential applicability to complex environmental matrices, particularly in complex clay-rich soils. Finally, direct detection may provide a methodological reference for MNP quantification in other matrices. For instance, in biological tissues, incomplete sample treatment (digestion followed by homogenization) may be sufficient for MNP quantification.

Theoretically, MNP are expected to accumulate preferentially in the topsoil, forming concentration hotspots that serve as persistent sources of exposure. Their detrimental effects are largely governed by bioavailability, which is closely linked to their redistribution from point- to non-point-source pollution following fragmentation and degradation. However, the redistribution behaviour and bioavailability of small MNP remain largely uncharacterised, representing a critical knowledge gap that current analytical methods have been unable to resolve. By enabling reliable quantification, direct detection will substantially improve our understanding of the fate of MNP in soil environments. It facilitates the investigation of the temporal and spatial dynamics of small-sized MNP, which is essential for assessing long-term soil exposure and evaluating terrestrial contributions to aquatic and atmospheric plastic pollution. Key transport processes, including bioturbation,[25, 56] agricultural practices,[57] surface runoff,[58] leaching,[59] and soil erosion [60] can now be quantified at the micrometre scale and even down to the nanoscale.[45] Moreover, mechanistic processes specific to small MNP, such as blocking effects and adsorption–desorption interactions with soil, can be investigated without being constrained by quantification limitations.[44]

582 Reliable quantification of small-sized MNP across distinct spatial distributions within
583 intact soil now makes it possible to isolate these mechanisms experimentally,
584 distinguish their relative contributions, and parametrise them for predictive modelling.
585 This represents a critical step toward understanding behaviour and bioavailability of
586 small MNP in terrestrial environments.

587 This framework may be extended to a posteriori labelling approaches, enabling the
588 quantification of environmentally derived MNP following appropriate labelling
589 strategies. Fluorescent labelling can be categorised into two types: (i) A priori labelling
590 (used in this study) involves labelling MNP with fluorescent dyes prior to their
591 deliberate introduction into matrices. This approach is typically applied to pure
592 monomers or pure MNP, thereby avoiding matrix interference during the labelling
593 process. (ii) A posteriori/direct labelling is a way to directly apply fluorescent dyes to
594 field samples or to unlabelled MNP extracted from such samples, thereby enhancing
595 MNP visualisation and detection.[29] Semi-automatic quantification of a posteriori
596 labelled MNP can be considered via calibration curves relating fluorescence area ratios
597 or particle abundance to MNP concentrations.[31, 50] However, a posteriori labelling
598 of MNP in soil often yields weak signals for particles $\leqslant$10 μm and hard to distinguish
599 small-sized MNP and co-labelling of soil organic matter.[61-63] Other challenges of a
600 posteriori labelling of MNP in soil include non-uniform fluorescence intensity and the
601 inability to label all MNP types.[61, 64] These limitations are most acute at the
602 nanoscale, where reliable a posteriori quantification of NP in complex soil matrices
603 remains largely unresolved. Addressing these constraints will require concurrent
604 advances in fluorescent labelling chemistry and detection methodology. Direct
605 detection provides a methodological foundation upon which to encourage the
606 development of in situ labelling strategies. When combined with complementary
607 spectroscopic identification techniques, such approaches hold potential to bridge the
608 gap between controlled laboratory systems and the quantification of native
609 environmental NP. Overall, this study establishes a quantitative framework for

investigating the behaviour, transport, and fate of small MNP in complex soil matrices, demonstrating that direct detection enables rapid, scalable, and broadly applicable quantification of small MNP without the requirement for labour-intensive separation.

Acknowledgements

The financial support of the Science Foundation Flanders (FWO) through the fundamental research project grant G0B6223N and the China Scholarship Council (CSC), China, for Yin Liu [CSC No. 202207565010] is gratefully acknowledged.

Reference

[1] Y. Li, J. Zhang, L. Xu, R. Li, R. Zhang, M. Li, C. Ran, Z. Rao, X. Wei, M. Chen, L. Wang, Z. Li, Y. Xue, C. Peng, C. Liu, H. Sun, B. Xing, L. Wang, Leaf absorption contributes to accumulation of microplastics in plants, Nature 641(8063) (2025) 666-673. https://doi.org/10.1038/s41586-025-08831-4.

[2] S. Allen, D. Allen, F. Baladima, V.R. Phoenix, J.L. Thomas, G. Le Roux, J.E. Sonke, Evidence of free tropospheric and long-range transport of microplastic at Pic du Midi Observatory, Nature Communications 12(1) (2021) 7242. https://doi.org/10.1038/s41467-021-27454-7.

[3] J. Zhao, R. Lan, H. Tan, J. Wang, Y. Ma, Q. Chen, F. Jiang, Z. Wang, B. Xing, Detection and characterization of microplastics and nanoplastics in biological samples, Nature Reviews Bioengineering (2025) 1-15.

[4] H. Sahai, A.M. Aguilera del Real, A. Alcayde, M.J.M. Bueno, C. Wang, M.D. Hernando, A.R. Fernández- Alba, Key insights into microplastic pollution in agricultural soils: A comprehensive review of worldwide trends, sources, distribution, characteristics and analytical approaches, TrAC Trends in Analytical Chemistry 185 (2025) 118176. https://doi.org/https://doi.org/10.1016/j.trac.2025.118176.

[5] A.E. Schwarz, S.M.C. Lensen, E. Langeveld, L.A. Parker, J.H. Urbanus, Plastics in the global environment assessed through material flow analysis, degradation and environmental transportation, Sci. Total Environ. 875 (2023) 162644. https://doi.org/10.1016/j.scitotenv.2023.162644.

[6] R. Lenz, K. Enders, T.G. Nielsen, Microplastic exposure studies should be environmentally realistic, Proceedings of the National Academy of Sciences 113(29) (2016) E4121-E4122. https://doi.org/doi:10.1073/pnas.1606615113.

[7] A.C.F. Möhrke, A. Haegerbaeumer, W. Traunspurger, S. Höss, Underestimated and ignored? The impacts of microplastic on soil invertebrates—Current scientific knowledge and research needs, Frontiers in Environmental Science Volume 10 - 2022 (2022). https://doi.org/10.3389/fenvs.2022.975904.

[8] J. Miao, W. Huang, R. Pan, K. Zhou, Research progress and hotspot analysis of soil microplastics: a bibliometrics-based review, Frontiers in Environmental Science Volume 11 - 2023 (2023). https://doi.org/10.3389/fenvs.2023.1297646.

[9] S. Gündoğdu, M.O. Akça, M. Gursoy, M. Yılmaz, X. Zhang, A. Rodríguez-Seijo, A. Bibi, M.L. Di Gioia, M. Velimirovic, Microplastics in soil: a comprehensive review of analytical techniques, Frontiers in Soil Science Volume 5 - 2025 (2025). https://doi.org/10.3389/fsoil.2025.1614075.

[10] X. Lim, Microplastics are everywhere—but are they harmful, Nature. 593(7857) (2021) 22-25. https://doi.org/10.1038/d41586-021-01143-3.

[11] M. Wang, H.-T. Fang, Q.-G. Tan, R. Ji, A.-J. Miao, Size-Dependent Toxicity of Polystyrene Nanoplastics to Tetrahymena thermophila: A Toxicokinetic–Toxicodynamic Assessment, Environmental Science & Technology 59(21) (2025) 10194-10203. https://doi.org/10.1021/acs.est.5c02150.

[12] Y. Kiyama, K. Miyahara, Y. Ohshima, Active uptake of artificial particles in the nematode Caenorhabditis elegans, Journal of Experimental Biology 215(7) (2012) 1178-1183.

https://doi.org/10.1242/jeb.067199.
[13] Y. Liu, J. Hu, J. Trap, J. Tan, N. Krekelbergh, P.N. Kusumawardani, R. Hoogenboom, A. Skirtach, S. De Neve, Microplastic transport in soil by nematodes, AGRIFOODPLAST, 2025.
[14] Y. Liu, R. Guo, S. Zhang, Y. Sun, F. Wang, Uptake and translocation of nano/microplastics by rice seedlings: Evidence from a hydroponic experiment, J Hazard Mater 421 (2022) 126700. https://doi.org/https://doi.org/10.1016/j.jhazmat.2021.126700.
[15] Y. Dong, M. Gao, W. Qiu, Z. Song, Uptake of microplastics by carrots in presence of As (III): Combined toxic effects, J Hazard Mater 411 (2021) 125055. https://doi.org/https://doi.org/10.1016/j.jhazmat.2021.125055.
[16] L. Li, Y. Luo, R. Li, Q. Zhou, W.J. Peijnenburg, N. Yin, J. Yang, C. Tu, Y. Zhang, Effective uptake of submicrometre plastics by crop plants via a crack-entry mode, Nature sustainability 3(11) (2020) 929-937.
[17] Q. Chen, A. Allgeier, D. Yin, H. Hollert, Leaching of endocrine disrupting chemicals from marine microplastics and mesoplastics under common life stress conditions, Environ. Int. 130 (2019) 104938. https://doi.org/10.1016/j.envint.2019.104938.
[18] L. Yang, Y. Zhang, S. Kang, Z. Wang, C. Wu, Microplastics in soil: A review on methods, occurrence, sources, and potential risk, Sci. Total Environ. 780 (2021) 146546. https://doi.org/10.1016/j.scitotenv.2021.146546.
[19] H. Dong, X. Wang, X. Niu, J. Zeng, Y. Zhou, Z. Suona, Y. Yuan, X. Chen, Overview of analytical methods for the determination of microplastics: Current status and trends, TrAC, Trends anal. chem. 167 (2023) 117261. https://doi.org/10.1016/j.trac.2023.117261.
[20] Y. Liu, et al. J Hazard Mater. 496 (2025) 139210. doi:10.1016/j.jhazmat.2025.139210. https://doi.org/https://doi.org/10.1016/j.jhazmat.2025.139210.
[21] G. Li, Z. Pei, Y. Li, R. Yang, P. Wang, Y. Liang, J. Zhang, Q. Zhang, G. Jiang, A high-precision, effective method for extraction and identification of small-sized microplastics from soil, Talanta. 272 (2024) 125802. https://doi.org/10.1016/j.talanta.2024.125802.
[22] M.G. Löder, H.K. Imhof, M. Ladehoff, L.A. Löschel, C. Lorenz, S. Mintenig, S. Piehl, S. Primpke, I. Schrank, C. Laforsch, Enzymatic purification of microplastics in environmental samples, Environmental science & technology 51(24) (2017) 14283-14292.
[23] M. Gniadek, A. Dąbrowska, The marine nano-and microplastics characterisation by SEM-EDX: The potential of the method in comparison with various physical and chemical approaches, Marine Pollution Bulletin 148 (2019) 210-216.
[24] T. Yang, J. Luo, B. Nowack, Characterization of Nanoplastics, Fibrils, and Microplastics Released during Washing and Abrasion of Polyester Textiles, Environmental Science & Technology 55(23) (2021) 15873-15881. https://doi.org/10.1021/acs.est.1c04826.
[25] S.Y. Chan, S.Y. Liu, R. Wu, W. Wei, J.K.-H. Fang, S.L. Chua, Simultaneous Dissemination of Nanoplastics and Antibiotic Resistance by Nematode Couriers, Environmental Science & Technology 57(23) (2023) 8719-8727. https://doi.org/10.1021/acs.est.2c07129.
[26] C. Harb, N. Pokhrel, H. Foroutan, Quantification of the Emission of Atmospheric Microplastics and Nanoplastics via Sea Spray, Environ Sci Tech Let 10(6) (2023) 513-519. https://doi.org/10.1021/acs.estlett.3c00164.
[27] S.W. Kim, Y.-J. An, Soil microplastics inhibit the movement of springtail species, Environment

International 126 (2019) 699-706. https://doi.org/https://doi.org/10.1016/j.envint.2019.02.067.
[28] C. Liu, Y. Jiao, J. Guo, B. Li, C. Gu, T. Qian, X. Liu, Tracing the entry process of submicrometre plastics in soybean sprouts by leaf-derived fluorescent carbon dots, J Hazard Mater 470 (2024) 134272. https://doi.org/https://doi.org/10.1016/j.jhazmat.2024.134272.
[29] Y. Liu, J. Li, B.V. Parakhonskiy, R. Hoogenboom, A. Skirtach, S. De Neve, Labelling of micro- and nanoplastics for environmental studies: state-of-the-art and future challenges, J Hazard Mater. 462 (2024) 132785. https://doi.org/10.1016/j.jhazmat.2023.132785.
[30] S. Liu, E. Shang, J. Liu, Y. Wang, N. Bolan, M. Kirkham, Y. Li, What have we known so far for fluorescence staining and quantification of microplastics: a tutorial review, Frontiers of Environmental Science & Engineering 16(1) (2022) 8.
[31] S. Sinha Ray, D. Zumr, F. Wilken, T. Dostál, P. Fiener, A cost-effective protocol for detecting fluorescent microplastics in arable soils to study redistribution processes, Polymer Testing 147 (2025) 108824. https://doi.org/https://doi.org/10.1016/j.polymertesting.2025.108824.
[32] USDA, Soil survey manual, Soil Survey Division Staff; Soil Conservation Service Volume Handbook 18, U.S. Department of Agriculture 2017.
[33] N.A. D'Ascanio, H. Almuhtaram, R.C. Andrews, Selection of an appropriate fluorescent reference material to assess microplastic recovery in natural waters, Microplastics and Nanoplastics 5(1) (2025) 18.
[34] S. Peneva, Q.N.P. Le, D.R. Munhoz, O. Wrigley, F. Wille, H. Doose, C. Halsall, P. Harkes, M. Sander, M. Braun, Microplastic analysis in soils: A comparative assessment, Ecotoxicology and Environmental Safety 289 (2025) 117428.
[35] M.A. Ali, X. Lyu, M.S. Ersan, F. Xiao, Critical evaluation of hyperspectral imaging technology for detection and quantification of microplastics in soil, J Hazard Mater 476 (2024) 135041. https://doi.org/https://doi.org/10.1016/j.jhazmat.2024.135041.
[36] Y. Seo, Y. Lai, G. Chen, J. Dearnaley, S. Wang, X. Liu, P. Song, Quantification of microplastics in agricultural soils by total organic carbon -solid sample combustion analysis, J Hazard Mater 490 (2025) 137841. https://doi.org/https://doi.org/10.1016/j.jhazmat.2025.137841.
[37] L. Xu, Y. Feng, A. Feng, Y. Yang, Y. Chen, B. Liu, N. Yang, W. Ma, Y. He, Z. Wu, Study on rapid quantitative detection of soil MPs based on terahertz time-domain spectroscopy, Analytical Chemistry 97(5) (2025) 2952-2962.
[38] F. Huang, W.-C. Yang, L. Ma, L. Chen, Y. Zeng, W. Dai, H. Jiang, C. Li, L. Fang, Micro(nano)plastic detection in soils: analytical techniques, AI applications, and future challenges, TrAC Trends in Analytical Chemistry 194 (2026) 118491. https://doi.org/https://doi.org/10.1016/j.trac.2025.118491.
[39] H. Hu, L. Qiang, S. Wei, J. Cheng, H. Pan, Z. Sun, Q. Li, R. Zhang, A "six-point S-shaped" sampling strategy based on micro-Raman spectroscopy enabling the rapid and accurate detection of small-sized microplastics in soil, J Hazard Mater 501 (2026) 140762. https://doi.org/https://doi.org/10.1016/j.jhazmat.2025.140762.
[40] S. Sujathan, A. El-Zein, Performance of analytical techniques for microplastic and nanoplastic quantification in the presence of clay, Water Res 288 (2026) 124716. https://doi.org/https://doi.org/10.1016/j.watres.2025.124716.
[41] S. Liu, P. Hoess, J. Ries, Super-resolution microscopy for structural cell biology, Annual review

of biophysics 51(1) (2022) 301-326.
[42] X. Hao, B. Ball, J. Culley, M. Carter, G. Parkin, Soil density and porosity, Soil sampling and methods of analysis 2(1) (2008) 743-759.
[43] Y. Luo, Y. Zhang, Y. Xu, X. Guo, L. Zhu, Distribution characteristics and mechanism of microplastics mediated by soil physicochemical properties, Science of The Total Environment 726 (2020) 138389. https://doi.org/https://doi.org/10.1016/j.scitotenv.2020.138389.
[44] K. Tsuchida, Y. Imoto, T. Saito, J. Hara, Y. Kawabe, Effect of solution pH on nanoplastic adsorption onto soil particle surface and the aggregation of soil particles, Science of the Total Environment 975 (2025) 178712.
[45] W.M. Heinze, D.M. Mitrano, E. Lahive, J. Koestel, G. Cornelis, Nanoplastic Transport in Soil via Bioturbation by Lumbricus terrestris, Environmental Science & Technology 55(24) (2021) 16423-16433. https://doi.org/10.1021/acs.est.1c05614.
[46] H. Blom, J. Widengren, Stimulated Emission Depletion Microscopy, Chemical Reviews 117(11) (2017) 7377-7427. https://doi.org/10.1021/acs.chemrev.6b00653.
[47] M.S.M. Al-Azzawi, M. Kunaschk, K. Mraz, K.P. Freier, O. Knoop, J.E. Drewes, Digest, stain and bleach: Three steps to achieving rapid microplastic fluorescence analysis in wastewater samples, Science of The Total Environment 863 (2023) 160947. https://doi.org/https://doi.org/10.1016/j.scitotenv.2022.160947.
[48] M. Shen, Y. Zhang, Y. Zhu, B. Song, G. Zeng, D. Hu, X. Wen, X. Ren, Recent advances in toxicological research of nanoplastics in the environment: A review, Environmental pollution 252 (2019) 511-521.
[49] J.C. Prata, J.R. Alves, J.P. da Costa, A.C. Duarte, T. Rocha-Santos, Major factors influencing the quantification of Nile Red stained microplastics and improved automatic quantification (MP-VAT 2.0), Science of The Total Environment 719 (2020) 137498. https://doi.org/https://doi.org/10.1016/j.scitotenv.2020.137498.
[50] R.A. Murray, A. Escobar, N.G. Bastús, P. Andreozzi, V. Puntes, S.E. Moya, Fluorescently labelled nanomaterials in nanosafety research: Practical advice to avoid artefacts and trace unbound dye, NanoImpact 9 (2018) 102-113.
[51] K.D. Sullivan, V. Gugliada, Fluorescence photobleaching of microplastics: A cautionary tale, Marine Pollution Bulletin 133 (2018) 622-625. https://doi.org/https://doi.org/10.1016/j.marpolbul.2018.06.019.
[52] S.Y. Lim, W. Shen, Z. Gao, Carbon quantum dots and their applications, Chemical Society Reviews 44(1) (2015) 362-381.
[53] K. Li, B. Liu, Polymer-encapsulated organic nanoparticles for fluorescence and photoacoustic imaging, Chemical Society Reviews 43(18) (2014) 6570-6597.
[54] O.S. Wolfbeis, An overview of nanoparticles commonly used in fluorescent bioimaging, Chemical Society Reviews 44(14) (2015) 4743-4768.
[55] Q. Zhang, X. Wang, J. Que, J. He, C. Peng, Y. Jiao, D. Zhao, D. Liu, H. Li, Z. Tang, Enhanced Stability and Luminescence Efficiency of CsPbBr3 PQDs via In Situ Growth and SiO2 Encapsulation in Surface-Functionalized Mesoporous Silica Nanospheres, Small 21(21) (2025) 2412581.
[56] M.C. Rillig, L. Ziersch, S. Hempel, Microplastic transport in soil by earthworms, Scientific reports 7(1) (2017) 1362.

[57] Y. Liu, M.C. Rillig, Q. Liu, J. Huang, M.A. Khan, X. Li, Q. Liu, Q. Wang, X. Su, L. Lin, Factors affecting the distribution of microplastics in soils of China, Frontiers of Environmental Science & Engineering 17(9) (2023) 110.
[58] N. Han, Q. Zhao, H. Ao, H. Hu, C. Wu, Horizontal transport of macro-and microplastics on soil surface by rainfall induced surface runoff as affected by vegetations, Science of the Total Environment 831 (2022) 154989.
[59] P. Yuan, X. Cao, L. Zhao, X. Xu, A. Romero-Freire, H. Qiu, Overlooked yet critical pathways for microplastics input to soil and groundwater system: Transport mechanisms and simulation predictions in landfill environments, Water Res 284 (2025) 124041. https://doi.org/https://doi.org/10.1016/j.watres.2025.124041.
[60] R. Rehm, T. Zeyer, A. Schmidt, P. Fiener, Soil erosion as transport pathway of microplastic from agriculture soils to aquatic ecosystems, Science of The Total Environment 795 (2021) 148774. https://doi.org/https://doi.org/10.1016/j.scitotenv.2021.148774.
[61] J. Zhang, H. Li, Y. Li, S. Li, Y. Xu, H. Li, Boron-doped carbon nanoparticles for identification and tracing of microplastics in “Turn-on” fluorescence mode, Chem Eng J 435 (2022) 135075. https://doi.org/https://doi.org/10.1016/j.cej.2022.135075.
[62] N. Expósito, J. Sierra, E. Martí, J. Folch, N. Ratola, M. Schuhmacher, J. Rovira, Detection of microplastic hotspots in beach sand for national surveys using fluorescence microscopy and infrared spectroscopy: Case study on the Catalan coast, Marine Pollution Bulletin 214 (2025) 117761. https://doi.org/https://doi.org/10.1016/j.marpolbul.2025.117761.
[63] C. Schür, S. Rist, A. Baun, P. Mayer, N.B. Hartmann, M. Wagner, When fluorescence is not a particle: the tissue translocation of microplastics in Daphnia magna seems an artifact, Environmental toxicology and chemistry 38(7) (2019) 1495-1503.
[64] E.G. Karakolis, B. Nguyen, J.B. You, C.M. Rochman, D. Sinton, Fluorescent dyes for visualizing microplastic particles and fibers in laboratory-based studies, Environ Sci Tech Let 6(6) (2019) 334-340.

Supplementary Information

Rapid quantification of fluorescent micro- and nanoplastics (≤2 μm) in soil

Table S1

Studies of fluorescent labelled small-sized microplastics and fluorescent nanoplastics (MNP) in sediment and soil.

MNP types	MNP shape	MNP size	Research purpose	Matrices	MNP quantification in Matrices	Reference
PS	Sphere	100 nm	Investigation of NP behaviour in interaction with nematodes	Loamy soil	No	[1]
PS	Sphere	20, 100 and 1000 nm	Investigation of MNP behavior in interaction with soil amoeba	Soil	No	[2]
PS	Sphere	0.5 and 1 µm	Method optimization for MP detection	Bentonite, montmorillonite, and kaolinite	Average percentage difference NTA: 0.5 µm (179 – 790%) FCM: 1 µm (11 – 39%) 0.5 µm (38 – 60%)	[3]
PS	Sphere	1.71 µm	Method optimization for MP identification	Quartz sand, sandy loam, silt loam, clay loam,	No	[4]
PS	Sphere	1 and 10 µm	Quantitatively Analyze Microplastic Transport in an Experimental Flume	Water and sediment	Recovery rate: Water (80–90%) Sediment (no quantification)	[5]
PS	Sphere	1,3, and 10 µm	Assessing the Behavior of Microplastics in Fluvial Systems	Water and sediment	Sediment (no quantification)	[6]
PS	Sphere	1, 10, and 20 µm	Transport of MP in saturated gravel and quartz sand	Natural gravel (medium and fine) and quartz sand (coarse and medium)	No	[7]

Literature was searched using the keywords fluorescent MP and fluorescent NP in combination with soil and sediment (search updated January 2026). Search results were manually screened, and studies not involving small-sized MNP were excluded.

Text S1 Magnetic nanoparticles preparation

Magnetic nanoparticles (15 ± 2 nm in size) were synthesized as follows[8] : a mixture of 5 ml 0.37 M $FeCl_3 \cdot 6H_2O$ and 5 ml 0.20 M $FeCl_2$ in 100 ml 0.15 M NaOH was sealed with parafilm, shaken for 30 min at 600 rpm on a magnetic stirrer, and decanted using a magnet to retain the magnetic nanoparticles at the bottom of the beaker. Magnetic nanoparticles underwent a stabilization process involving four cycles of citric acid washing, utilizing 15 ml of citric acid in each cycle. Subsequently, three rounds of washing with 15 ml deionized water were performed. Then, the magnetic nanoparticles were re-suspended in 5 ml of deionized water. The concentration of magnetic nanoparticles (15.55 mg/ml) was determined gravimetrically after evaporation of a 1 ml subsample in an oven at 90°C.

Text S2 Density separation of 2 µm MP from loamy sand

Two concentrations of 2 µm MP (100 mg/kg and 10 mg/kg) were separately mixed with 0.1 g of loamy sand and 2 ml of 30% H_2O_2 (three replicates, n=3). The mixture was subsequently incubated at 70 °C for 10 h, until the soil particles appeared grayish-white and bubbles were no longer observed in the suspension. Then, 3 ml saturated NaCl was added, followed by ultrasonication (Ultrasonic Processor GEX 750) for a duration of 2.5 min at the maximum energy setting of 2500 J/mL, with a pulse interval of 5 s. After ultrasonication, the ultrasonic probe in soil suspension was rinsed with 2 ml of saturated NaCl solution to minimise MP loss during the process. The rinsing solution was added to the sonicated mixture. The mixture was transferred to a centrifuge tube, and the glass bottle was rinsed three times with 1 ml of saturated NaCl solution to ensure that no residues remained. The mixture in the centrifuge tube was mixed using ultrasonication (3 min) and manual shaking, followed by centrifugation at 3000 rpm for 8 min. After centrifugation, the supernatant was collected, weighed, and homogenised. Subsequently, 1/20 of the total supernatant volume was extracted and filtered. This 1/20 ratio was adopted to maintain consistency in the proportion of the measured sample relative to the total sample, in alignment with the magnetic separation and direct

measurement methods. The solution was finally diluted to a constant volume of 10 mL, and 0.5 mL was taken for filtration and measurement. The filtration procedure and fluorescence measurements were identical as for direct detection (section 2.2.2 and 2.2.3). The entire procedure, encompassing ultrasonication, density separation, and fluorescence microscopy-based quantification, was performed in triplicate, and the spiked recovery rates obtained from each separation step were summed to calculate the total recovery rate.

Text S3 Magnetic separation of 2 μm MP from loamy sand

MP were mixed with 0.1 g of loamy sand at concentrations of 100 and 10 mg/kg, in three replicates (n=3), 5 mL 0.1 M NaCl was added, and the mixture was incubated at 90 °C for 1.5 h. Once removed from the over, 0.7 mg of magnetic nanoparticles were added immediately to the hot samples, which were then shaken at 300 rpm for 20 min. After cooling, the mixture was transferred to a 15 mL glass centrifuge tube with a magnet positioned adjacent to it. The settled soil particles were removed using a 5 mL pipette and transferred to a fresh glass centrifuge tube to undergo a second magnetic separation. The two remaining (magnetically extracted) fractions were combined and adjusted to a final volume of 10 mL with 0.1 M NaCl. A 0.5 mL aliquot was then taken and filtered through a 0.45 μm filter paper. The filtration procedure and fluorescence measurements were identical as for direct detection (section 2.2.2 and 2.2.3). The above steps, including incubation, shaking, magnetic separation, filtration and fluorescence microscopy-based quantification, was performed in triplicate, and the spiked recovery rates obtained from each separation step were summed to calculate the total recovery rate.

Text S4 Data acquisition protocols used for establishing calibration curve (Table 2, IIA)

To optimise the data acquisition protocol for establishing a calibration curve between fluorescence area ratio and MP concentration, a series concentrations of 2 μm

MP (0.01, 0.05, 0.1, 0.5, 1, 5, 10, 50, 100, 500, and 1000 mg/kg) were individually mixed with 0.1 g of loamy sand. The detection was done following the methodology described in section 2.2.2 and section 2.2.3. The effect of the number of replicate samples (1, 2, and 3), the number of subsamples per replicate (1, 2, and 3), and the number of images per filter (10, 20, 30, 40, and 50) on the Pearson correlation coefficient (r) of the calibration curve using a resampling approach.

The r between the base-10 logarithm of MP concentration and fluorescence area ratio were calculated using three different sampling methods (illustrated in Figure S1):

i) A combination of 3 replicate samples each subsampled in triplicate, i.e. actual analysis of 9 subsamples (fluorescent area ratios for each subsample obtained from 50 images, as above). The area ratios for these 9 subsamples (i.e. 9 data points) were averaged for each of the 11 concentrations to obtain A_1–A_{11}. MP concentrations were converted to percentage (C_1–C_{11}) to obtain dimensionless values. Pearson correlation coefficients were calculated between the base-10 logarithm of the fluorescence area ratios ($\log_{10} A_1$–A_{11}) and the base-10 logarithm of MP concentrations ($\log_{10} C_1$–C_{11}).

ii) 3 replicate samples subsampled only once: a single subsample was randomly selected from each of the three samples. A total of three fluorescence area ratios (3 samples × 1 subsamples = 3 data points) for each 11 concentration were averaged to obtain B_1–B_{11}. The averaged fluorescence area ratios were converted to their base-10 logarithms ($\log_{10} B_1$–B_{11}), and then correlated with the base-10 logarithms of MP concentrations ($\log_{10} C_1$–C_{11}) to calculate the r values.

iii) 1 replicate sample subsampled only once: At each concentration, a single subsample was selected (D_1–D_{11}). The base-10 logarithm of the fluorescence area ratios at the 11 MP concentrations ($\log_{10} D_1$–D_{11}) was correlated with the base-10 logarithm of MP concentrations ($\log_{10} C_1$–C_{11}) to calculate the r values.

To assess the effect of the number of input images on the Pearson correlation, 40 (12.73% of the total soil layer area), 30 (9.55%), 20 (6.37%), and 10 (3.18%) images were randomly selected from the total of 50 images. Image subsets of varying sizes

were randomly sampled in triplicate to generate distinct image-derived datasets. Given the multiple possible permutations in selecting replicate samples, subsampling ratios, and image counts across the 11 MP concentration levels, the corresponding sampling method within image-derived datasets was applied 25 times via random sampling without replacement, yielding 25 distinct r values. These values were then averaged to assess the accuracy and stability of direct detection under different resampling approaches. The lowest detected concentration (LDC) for each data acquisition protocol was defined as the lowest concentration that could be detected in all replicate sampling. Specifically, in repeated sampling calculations, if a zero value of the fluorescence area ratio occurred at a given MP concentration in (at least) one replicate, that concentration and all lower concentrations were excluded from the correlation analysis.

The results of the above method comparison indicate that the direct detection method is highly robust, as demonstrated by the consistently strong correlations between MP concentrations and fluorescence area ratios (r = 0.993–0.997) across different data acquisition protocols (Table S2). A combination of 3 replicate samples each subsampled in triplicate and 50 images per filter paper (the largest data volume in this study) yielded a calculated r = 0.996. The r and its stability were affected by both the number of replicate samples and images. Increasing the number of replicate samples from 1-replicate sample ×1-subsample to 3-replicate samples ×1-subsample, a relative improvement in both the r and standard error was observed. Increasing the number of images can also improve both the r and decrease the LDC. For the 1-replicate sample × 1-subsample approach, acquiring at least 30 images is necessary to improve measurement stability and ensure reliable quantification down to 0.05 mg/kg. At 0.01 mg/kg, however, MP were detected in only 3 of the 450 images analysed (3-replicatesamples × 3 subsamples × 50 images). Increasing subsamples from 3-samples × 1-subsamples to 3-replicate samples × 3-subsample had no increase in the r. Therefore, the 1-replicate sample × 1-subsample approach combined with ⩾30 images per filter offers a more time-efficient option, whereas the 3-replicate sample × 1-subsample

strategy provides greater stability. We therefore established the method for obtaining the calibration curve. For each MP concentration, a single replicate sample with one subsample was prepared, and 30 images per filter were initially acquired. If fewer than two fluorescent particles were observed within the initial 30 images, the number of images was increased to 150 to improve detection accuracy at low MP concentrations. The mean fluorescence area ratio per image was calculated, and a linear relationship between the base-10 logarithms of fluorescence area ratio and MP concentration was established to construct the calibration curve.

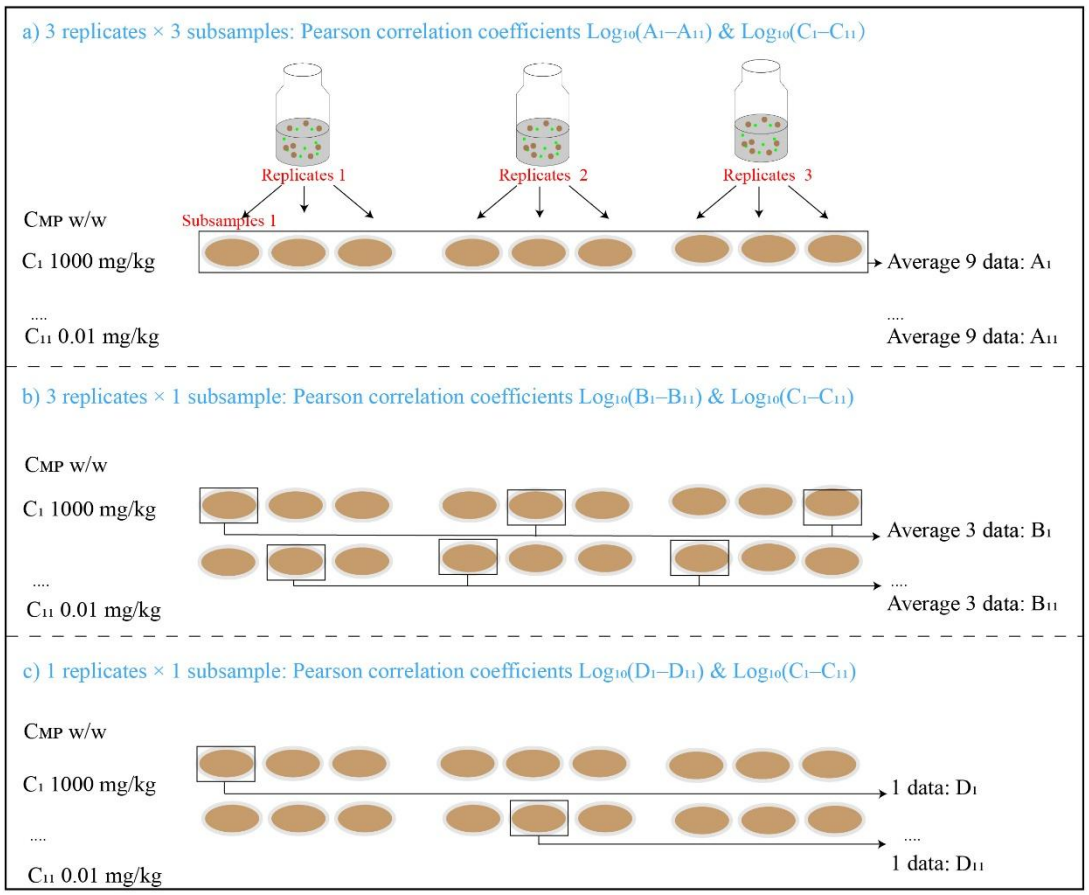

Figure S1. Schematic illustration of various data acquisition methods and the corresponding steps for calculating the Pearson correlation coefficient

Table S2

Pearson correlation coefficient (r) between fluorescence area ratios and MP concentrations, and corresponding detection limits under various data acquisition methods.

Images amount (Percentage of total filter)	r (3-replicate samples ×3-subsamples)	LDC (mg/kg)	n	r (3-replicate samples ×1-subsample)	n	LDC (mg/kg)	r (1-replicate sample ×1-subsample)	LDC (mg/kg)	n
50 images (15.92%)	0.996	0.01	1	0.997±0.001	25	0.05	0.996±0.001	0.05	25
40 images (12.73%)	0.996±0.001	0.01	25	0.997±0.001	25	0.05	0.995±0.004	0.05	25
30 images (9.55%)	0.996±0.002	0.01	25	0.997±0.001	25	0.05	0.995±0.003	0.05	25
20 images (6.37%)	0.994±0.001	0.01	25	0.996±0.002	25	0.05	0.994±0.003	0.1	25
10 images (3.18%)	0.997±0.001	0.05	25	0.996±0.002	25	0.05	0.993±0.003	0.1	25

The lowest detected concentration (LDC) refers to the lowest concentration of MP that can be detected by every times sampling approaches. n represents the total number of observations used to calculate the mean r.

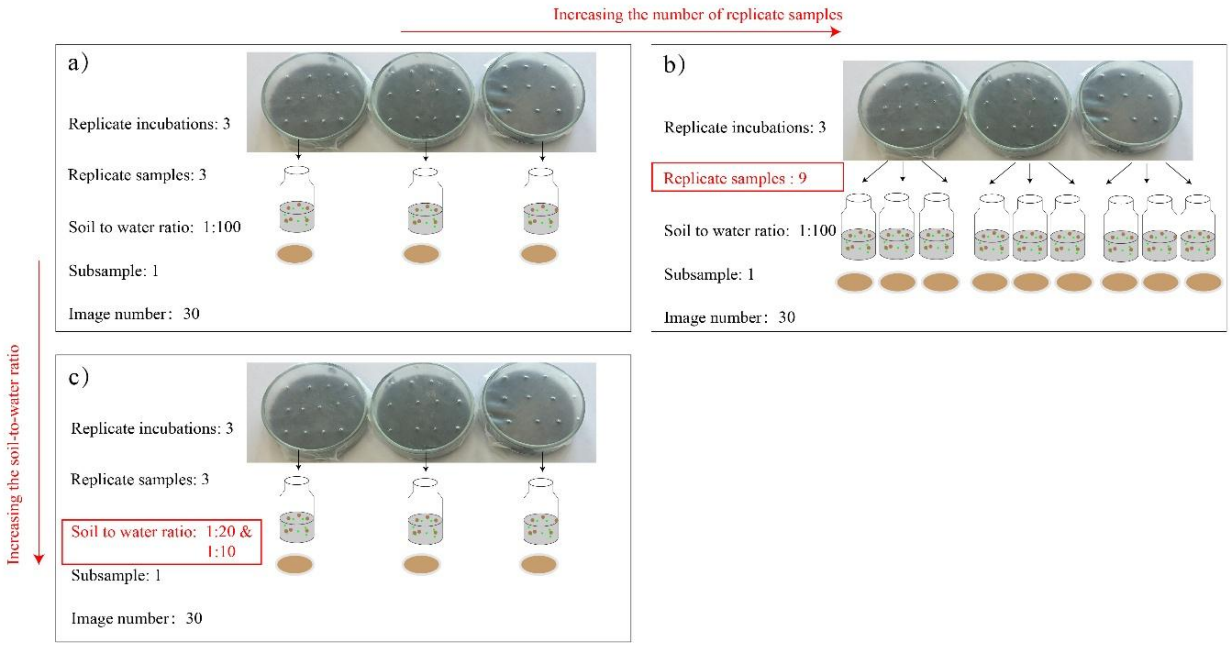

Figure S2. Schematic illustration of the expanded calibration-based quantification framework (a) and further experiments aimed at improving analytical accuracy through increasing the number of replicate samples (b) and the soil-to-water ratio (c).

Text S5 Evaluation of the calibration-based quantification

To evaluate whether increasing the number of replicate samplings (0.1 g of soil sampled from 5 g of incubated soil) helps to minimise detection errors using the calibration curve, two additional replicate samples were collected from each MP replicate and analysed. We further investigated whether increasing the soil-to-water ratio during dispersion would affect validation accuracy. The initial soil-to-water ratio (1:100) was adjusted to 20:1 and 10:1 (Table S3). The measurement and calculation followed the procedures outlined in section 2.3.2.

To quantify prediction errors, mean absolute error (MAE), root mean square error (RMSE), and the average symmetric mean absolute percentage error (SMAPE) were calculated based on calibration curve using the following formula:

$$\mathrm{MAE} = \frac{1}{n}\sum_{i=1}^{n}|y_i - \hat{y}_i|$$

$$\mathrm{RMSE} = \sqrt{\frac{1}{n}\sum_{i=1}^{n}(y_i - \hat{y}_i)^2}$$

$$\mathrm{SMAPE} = \frac{100\%}{n}\sum_{i=1}^{n}\frac{|y_i - \hat{y}_i|}{(|y_i| + |\hat{y}_i|)/2}$$

Where n is the number of samples, at, $\hat{y}_i$ is the predicted MP concentration. y_i is the observed/added MP concentration.

Table S3

Validation of calibration curve at different soil-to-water ratios after 15 days of incubation. Calculation based on soil with a particle density of 2.65 g/cm³

MP concentration mg/kg	Soil (g)	Water (mL)	Soil to water ratio	Suspension volume (mL)	Tested suspension volume (μL)
100	0.1	10	1:100	10.0377	500
	0.5	10	1:20	10.1887	101.6
	1	10	1:10	10.3774	51.8
1	0.1	10	1:100	10.0377	500
	0.5	10	1:20	10.1887	101.6
	1	10	1:10	10.3774	51.8

Table S4

Error analysis of different sampling numbers and soil-to-water ratios based on the 15-day incubation experiment.

MP concentrations		1 mg/kg			100 mg/kg		
		MAE (mg/kg)	RMSE (mg/kg)	SMAPE (%)	MAE (mg/kg)	RMSE (mg/kg)	SMAPE (%)
Replicate samples	3	0.18	0.19	17	23	27	28
	9	0.16	0.19	15	32	34	39
Soil to water ratio	1:100	0.18	0.19	17	23	27	28
	1:20	0.24	0.31	21	34	34	41
	1:10	0.21	0.23	24	48	48	63

Table S5

Correlation analysis of R^2 and the basic properties of the soils.

	The total fluorescence area ratio	Sand %	Silt %	Clay %	SOC %	pH-KCl
R^2	0.578	0.623	–0.717	–0.006	–0.570	–0.761*
The total fluorescence area ratio	1	0.964**	–0.863*	–0.581	–0.284	–0.888**
Sand %		1	–0.930**	–0.521	–0.457	–0.833*
Silt %			1	0.171	0.691	0.794*
Clay %				1	-0.378	0.389
SOC %					1	0.279

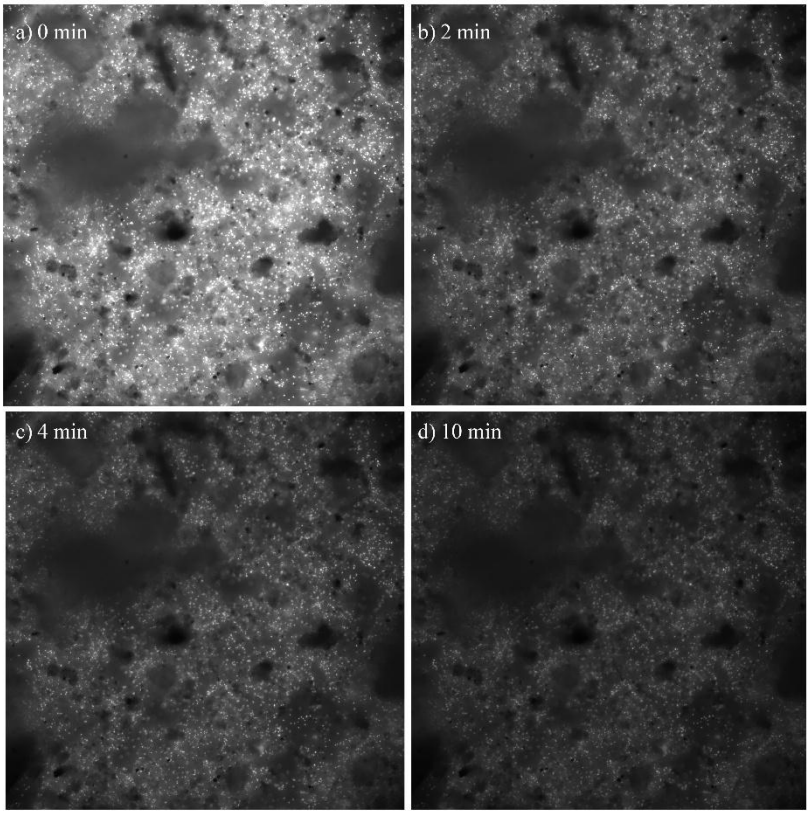

Figure S3. Fluorescence images of loamy sand at 1000 mg/kg NP concentration. a–d correspond to continuous exposure durations of 0, 2, 4, and 10 min, respectively, under an exposure time of 30 ms and excitation wavelength level 3

Reference

(1) Chan, S. Y.; Liu, S. Y.; Wu, R.; Wei, W.; Fang, J. K.-H.; Chua, S. L. Simultaneous Dissemination of Nanoplastics and Antibiotic Resistance by Nematode Couriers. *Environmental Science & Technology* **2023**, *57* (23), 8719-8727. DOI: 10.1021/acs.est.2c07129.

(2) Zhang, S.; He, Z.; Wu, C.; Wang, Z.; Mai, Y.; Hu, R.; Zhang, X.; Huang, W.; Tian, Y.; Xia, D. Complex bilateral interactions determine the fate of polystyrene micro-and nanoplastics and soil protists: implications from a soil amoeba. *Environmental Science & Technology* **2022**, *56* (8), 4936-4949.

(3) Sujathan, S.; El-Zein, A. Performance of analytical techniques for microplastic and nanoplastic quantification in the presence of clay. *Water Res* **2026**, *288*, 124716. DOI: https://doi.org/10.1016/j.watres.2025.124716.

(4) Krekelbergh, N.; Li, J.; Kusumawardani, P. N.; Liu, Y.; Hu, J.; Sleutel, S.; Parakhonskiy, B.; Hoogenboom, R.; De Neve, S.; Skirtach, A. Comparison of Raman and fluorescence microscopy for identification of small (< 2 μm) microplastics in soil. *Environmental Pollution* **2025**, *374*, 126204. DOI: https://doi.org/10.1016/j.envpol.2025.126204.

(5) Boos, J.-P.; Gilfedder, B. S.; Frei, S. Tracking Microplastics Across the Streambed Interface: Using Laser-Induced-Fluorescence to Quantitatively Analyze Microplastic Transport in an Experimental Flume. *Water Resources Research* **2021**, *57* (12), e2021WR031064. DOI: https://doi.org/10.1029/2021WR031064.

(6) Boos, J.-P.; Dichgans, F.; Fleckenstein, J. H.; Gilfedder, B. S.; Frei, S. Assessing the Behavior of Microplastics in Fluvial Systems: Infiltration and Retention Dynamics in Streambed Sediments. *Water Resources Research* **2024**, *60* (2), e2023WR035532. DOI: https://doi.org/10.1029/2023WR035532.

(7) Ameen, A.; Stevenson, M. E.; Kirschner, A. K. T.; Jakwerth, S.; Derx, J.; Blaschke, A. P. Fate and transport of fragmented and spherical microplastics in saturated gravel and quartz sand. *Journal of Environmental Quality* **2024**, *53* (5), 727-742. DOI: https://doi.org/10.1002/jeq2.20618.

(8) German, S. V.; Inozemtseva, O. A.; Markin, A. V.; Metvalli, K.; Khomutov, G. B.; Gorin, D. A. Synthesis of magnetite hydrosols in inert atmosphere. *Colloid Journal.* **2013**, *75* (4), 483-486. DOI: 10.1134/S1061933X13040042.